NTNU

Norwegian University of
Science and Technology

Investigation of wave transformation and breaking processes in the coastal zone using REEF3D

Mohamed Elakel

Coastal and Marine Engineering and Management
Submission date: July 2018
Supervisor: Hans Sebastian Bihs, IBM
Co-supervisor: Arun Kamath, IBM
Ankit Aggarwal, IBM

Norwegian University of Science and Technology
Department of Civil and Environmental Engineering

ERASMUS +: ERASMUS MUNDUS MOBILITY PROGRAMME

Master of Science in

COASTAL AND MARINE ENGINEERING AND MANAGEMENT

CoMEM

INVESTIGATION OF WAVE TRANSFORMATION AND BREAKING PROCESSES IN THE COASTAL ZONE USING REEF3D

Norwegian University of Science and Technology
9 July 2018

Mohamed Elakel

The Erasmus+: Erasmus Mundus MSc in Coastal and Marine Engineering and Management is an integrated programme including mobility organized by five European partner institutions, coordinated by Norwegian University of Science and Technology (NTNU).

The joint study programme of 120 ECTS credits (two years full-time) has been obtained at two or three of the five CoMEM partner institutions:

- Norges Teknisk- Naturvitenskapelige Universitet (NTNU) Trondheim, Norway
- Technische Universiteit (TU) Delft, The Netherlands
- Universitat Politècnica de Catalunya (UPC). BarcelonaTech. Barcelona, Spain
- University of Southampton, Southampton, Great Britain
- City University London, London, Great Britain

During the first three semesters of the programme, students study at two or three different universities depending on their track of study. In the fourth and final semester an MSc project and thesis has to be completed. The two-year CoMEM programme leads to a multiple set of officially recognized MSc diploma certificates. These will be issued by the universities that have been attended by the student. The transcripts issued with the MSc Diploma Certificate of each university include grades/marks and credits for each subject.

Information regarding the CoMEM programme can be obtained from the programme coordinator:

Øivind A. Arntsen, Dr.ing.
Associate professor in Marine Civil Engineering
Department of Civil and Environmental Engineering
NTNU Norway
Mob.: +4792650455 Fax: + 4773597021
Email: oivind.arntsen@ntnu.no

CoMEM URL: https://www.ntnu.edu/studies/mscomem

CoMEM Thesis

This thesis was completed by:
Mohamed Elakel

Under supervision of:
Hans Bihs, Associate professor, NTNU
Arun Kamath, Postdoc, NTNU
Ankit Aggarwal, PhD, NTNU

As a requirement to attend the degree of
Erasmus+: Erasmus Mundus Master in Coastal and Marine Engineering and Management (CoMEM)

Taught at the following educational institutions:

Norges Teknisk- Naturvitenskapelige Universitet (NTNU)
Trondheim, Norway

Technische Universiteit (TU) Delft
Delft, The Netherlands

At which the student has studied from August 2016 to July 2018.

NTNU
Faculty of Engineering Science and Technology
Department of Civil and Transport Engineering

MASTER THESIS

(TBA4920 Marine Civil Engineering, Master Thesis)

Spring 2018
for
Mohamed Elakel

Investigation of wave transformation and breaking processes in the coastal zone using REEF3D

Etterforskning av bølge transformasjon og bryting prosesser i kyst områder med REEF3D

BACKGROUND

The coastal zone is a major contributor in shaping the economies and the communities of many countries around the globe. Around half of the population live or work within one or two hundred kilometer of the coastline. In addition to that, industries and activities like shipping, trading, fishing and aquaculture is affected by any changes to the coastal zone. Therefore, it is very important to know the dynamics of the forcing on the system and the response of the system to better evaluate choices related to the development of the coastal areas.
In order to evaluate the forcing, a thorough understanding of the physical phenomenon is needed. The processes that happen to the waves while approaching the nearshore, like shoaling, refraction and wave breaking must be assessed in order to accurately predict wave forces of the coastline and the coastal structures.
The breaking process involves many complex parameters and breaking waves may occur at the site depending on the water depth, wave height, seabed slope, wave period and steepness. An exact numerical modeling of wave breaking process is still highly challenging due to the strong non-linear air-sea interaction at the free surface, air entrainment, and strong turbulent production by breaking is highly dissipative.

TASK DESCRIPTION

Description of task

The Master thesis task involves numerical modelling of wave propagation and transformation in the coastal region. This includes wave shoaling, wave breaking and wave run up on coasts under different wave conditions. The candidate is expected to carry out a thorough literature review to obtain the state-of-the-art on wave breaking and shoaling in the coastal zone over natural topography. The simulations of wave shoaling, breaking and transformation will be carried out using the open-source hydrodynamic

model REEF3D developed at the Department of Civil and Environmental Engineering at NTNU Trondheim. REEF3D will firstly be used to model a case which is done in a wave tank in the lab under monitored conditions. The shoaling and breaking of waves will be captured through the numerical model and results will be compared to the lab measurements. After that, the usage of REEF3D will be extended to an irregular bottom, the results of the water surface elevation using the numerical model will be compared to large scale measurements. The inputs, outputs and different aspects of the modelling process will be discussed and breaking and shoaling parameters will be investigated to help in understanding many field problems in the nearshore coastal zone.

Objectives

The Masters' thesis work will be carried out with the following objectives:

- Simulation of plunging breaking waves on a constant slope
- Study the run up on coasts under different wave conditions
- Simulation of wave shoaling and transformation on irregular bottom
- Simulation of wave breaking on irregular bottom

Subtasks and research questions

As an introduction, the candidate must show that she/he has the advanced knowledge of the field of numerical modelling of wave hydrodynamics using CFD based numerical wave tanks with respect to theory and methods with in general. The candidate should review literature, replicate the experimental setups from literature numerically and compare the numerical and experimental results. He should demonstrate the ability to validate a numerical model with careful study of the experiments and execution of the numerical model. It is expected that the candidate extends upon the study with further research using REEF3D. After the processes of wave shoaling and wave breaking on a regular bottom are studied, the candidate will simulate and analyse the wave transformation processes on irregular bottom and natural topography.

General about content, work and presentation

The text for the master thesis is meant as a framework for the work of the candidate. Adjustments might be done as the work progresses. Tentative changes must be done in cooperation and agreement with the professor in charge at the Department. In the evaluation thoroughness in the work will be emphasized, as will be documentation of independence in assessments and conclusions. Further, the presentation (report) should be well organized and edited; providing clear, precise and orderly descriptions without being unnecessary voluminous.

The report shall include:

- Standard report front page (from DAIM, http://daim.idi.ntnu.no/)
- Title page with abstract and keywords. (template on: http://www.ntnu.no/bat/skjemabank)
- Preface
- Summary and acknowledgement. The summary shall include the objectives of the work, explain how the work has been conducted, present the main results achieved and give the main conclusions of the work.
- Table of content including list of figures, tables, enclosures and appendices.
- A list explaining important terms and abbreviations should be included.
- List of symbols should be included
- The main text.
- Clear and complete references to material used, both in text and figures/tables. This also applies for personal and/or oral communication and information.
- Thesis task description (these pages) signed by professor in charge as Attachment 1.
- The report musts have a complete page numbering.

The thesis can as an alternative be made as a scientific article for international publication, when this is agreed upon by the Professor in charge. Such a report will include the main points as given above, but where the main text includes both the scientific article and a process report.

Submission procedure

Procedures relating to the submission of the thesis are described in IVT faculty webpage:
http://www.ntnu.edu/ivt/master-s-thesis-regulations

On submission of the thesis the candidate shall submit to the professor in charge a CD/DVD('s) or a link to a net-cloud including the report in digital form as pdf and Word (or other editable form) versions and the underlying material (such as data collection, time series etc.).

Documentation collected during the work, with support from the Department, shall be handed in to the Department together with the report.

According to the current laws and regulations at NTNU, the report is the property of NTNU. The report and associated results can only be used following approval from NTNU (and external cooperation partner if applicable). The Department has the right to make use of the results from the work as if conducted by a Department employee, as long as other arrangements are not agreed upon beforehand.

Start and submission deadlines

The work on the Master Thesis starts on 12.2.2018

The thesis report as described above shall be submitted digitally in DAIM at the latest (date:) 09/07/2018 at 23:59:59.

Professor in charge: **Hans Bihs**

Other supervisors: **Arun Kamath, Ankit Aggarwal**

Trondheim, 12.2.2018

Professor in charge (sign)

NORWEGIAN UNIVERSITY OF SCIENCE AND TECHNOLOGY
DEPARTMENT OF CIVIL AND ENVIRONMENTAL ENGINEERING

Report Title:	Date: 09/07/2018			
Investigation of wave transformation and breaking processes in the coastal zone using REEF3D	Number of pages (incl. appendices):			
	Master Thesis	X	Project Work	

Name:

Mohamed Elakel

Professor in charge/supervisor:

Prof. Hans Bihs

Other external professional contacts/supervisors:

Arun Kamath, Ankit aggarwal

Abstract:

Several human activities and industries that contribute in shaping the communities and economies around the world are located in the coastal zone. Therefore, it is very crucial to understand the behaviour of the coastal system to better evaluate the design choices related to the treatment of these areas.

Thanks to the rapid technological development in the computational domain, it is now possible to simulate the evolution of waves numerically to a great accuracy and evaluate their effects on the structures. In this thesis, the main goal is to numerically model the evolution and breaking of waves using CFD model REEF3D and compare the results to field data obtained with Lidar and ADV sensors.

The novelty in this work lies in giving more accuracy in the prediction of the behaviour of the waves by employing a CFD model which solves Naiver-stokes equations, in contrast to using phase-based models or shallow water equation models.

The complexity of simulating waves in the field lies in the numerous contributing variables that can not be controlled in a measurement campaign. The irregularity of the phases, directions and frequencies of the waves and their evolution on a three-dimensional irregular bathymetry increase the difficulty of the task. Consequently, some bench-marking simpler cases will be investigated first and will be compared to laboratory monitored experiments to have confidence in the CFD model and to understand the underlying physics of the problem.

In the first case, the run-up of a solitary wave on a constant slope is compared to a laboratory experiment. In the second case, regular waves will be imposed on a constant slope and the plunging breaking behaviour will be compared to a laboratory experiment. The third case will investigate the behaviour of irregular waves on an experimental irregular slope and lastly the field case will be tackled and compared to field measurements. Different Numerical options will be tested and results will be compared to arrive to the highest accuracy possible.

Keywords:

1. COMEM
2. REEF3D
3. Regular/ Irregular Breaking waves
4. Lidar field data and CFD comparison

Investigation of wave transformation and breaking processes in the coastal zone using REEF3D

A Thesis
submitted to the Faculty of Civil Engineering
at the Norwegian University of Science and Technology
in partial fulfillment of the requirements for the degree of

Master of Science

by

Mohamed Elakel

Acknowledgement

First and foremost, I would like to praise God for his blessings and for giving me this wonderful opportunity to be part of this master program.

I thank my supervisors, Dr.Hans Bihs, for allowing me to participate and contribute to this exciting topic and Dr.Arun Kamath for his support and continuous help during the execution of the thesis. I would like to thank my parents and my sister for encouraging me to be the best version of my self.

I would also like to extend my gratitude to all professors who have educated me during my two-year COMEM program in NTNU and TU Delft. I especially thank Dr.Raed Lubbad and Dr. Oivind Arnsten for their support through the two years.

This masters thesis research was supported in part by computational resources provided by the Norwegian Metacenter for Computational Science, NOTUR under project number NN2620K.

Abstract

Several human activities and industries that contribute in shaping the communities and economies around the world are located in the coastal zone. Therefore, it is very crucial to understand the behaviour of the coastal system to better evaluate the design choices related to the treatment of these areas.

Thanks to the rapid technological development in the computational domain, it is now possible to simulate the evolution of waves numerically to a great accuracy and evaluate their effects on the structures. In this thesis, the main goal is to numerically model the evolution and breaking of waves using the open-source CFD model REEF3D and compare the results to field data obtained with Lidar and ADV sensors.

The novelty of this work lies in modelling a large scale field case with a CFD model in contrast to shallow water or phase-based models. Moreover, the accuracy of the results is improved by using wave reconstruction method in the generation of the incoming wave boundary and the application of non-uniform grids.

The complexity of simulating waves in the field lies in the numerous contributing variables that can not be controlled in a measurement campaign. The irregularity of the phases, directions and frequencies of the waves and their evolution on a three dimensional irregular bathymetry increase the difficulty of the task. Consequently, some bench-marking simpler cases will be investigated first and will be compared to laboratory monitored experiments to have confidence in the CFD model and to understand the underlying physics of the problem.

In the first case, the run-up of a solitary wave on a constant slope is compared to a laboratory experiment. In the second case, regular waves will be imposed on a constant slope and the plunging breaking behaviour will be compared to a laboratory experiment. The third case will investigate the behaviour of irregular waves on an experimental irregular slope and lastly the field case will be tackled and compared to field measurements.

Contents

List of Figures

Chapter 1

Introduction

1.1 Motivation

The coastal zone is a major contributor in shaping the communities and the economies around the world. In fact, around 40% of the population lives within 100 km of the coastline [35]. Activities and industries close to the coast include: shipping, trading, fishing and recreation. The ocean however, imposes forces that can hinder these activities, for instance:

- Propagation of waves in harbours can affect the mooring of vessels and can cause the snapping of mooring lines, which can damage the ships or increase the traffic time and eventually negatively impact the economy.
- Sediment transport by waves can cause sedimentation of ports and harbours basins, thus reducing the required navigation depth for the ships and necessitating dredging.
- Waves exert forces on coastal structures such as breakwaters or wind turbines close to the coast and can cause their failure if not designed properly.
- Extreme waves and storms can cause erosion of the dunes in coastal areas which result in the damage of recreational areas and can cause flooding in extreme cases.
- Long shore transport induced by wave breaking can also contribute to erosion of beaches.

Therefore, it is very crucial to understand the dynamics of the forcing and the response of the system to better evaluate choices related to the development of the coastal areas.

Waves undergo several changes to their structure as they approach the coast from deep water because of the change in bathymetry. The reduction in water depth leads the waves to reduce in length and increase in height, also known as shoaling. They also refract so that the wave crests become parallel to the shoreline. This happens as a result of the change in water depth and thus speed in different locations along the wave crest. Diffraction of waves occurs when waves meet obstacles or breakwaters close to harbours. The diffracted wave is a result of the transmission of a part of the incident energy to the shadow zone behind the obstacle.

In addition to the processes discussed, waves undergo a very important transformation in the coastal zone, which is breaking. Breaking of waves (described in detail in section 1.2), lead to the dissipation of wave energy on the beach and is associated with a lot of dynamic behaviour, turbulence, air entrainment and mixing of sediments. Moreover, it is the main driving force for the longitudinal transport which can cause erosion in many locations.

The goal of this thesis is to improve the understanding of the evolution of waves as they approach the coast and specifically the process of wave breaking and model it numerically. This will be achieved by performing numerical simulations of the four following cases:

- Case 1: The run up process of a tsunami wave on a plane slope and comparison with laboratory measurements.
- Case 2: The behaviour of plunging breaking waves on a plane slope and comparison with laboratory measurements.
- Case 3: The evolution of irregular wave breaking on an irregular slope and comparison with laboratory measurements.
- Case 4: The evolution of irregular waves on natural topography and comparison with field measurements.

1.2 Background

Waves are generated in deep waters by wind. When these waves propagate in shallower areas, their structure gets modified by the changes in the bottom. This causes the crest to sharpen, the trough to be more flat, the waves become too steep and eventually break as a result of instability.

Since the prediction of wave breaking characteristics, location and forces are very important, many experimental and theoretical studies have been carried out to identify the wave kinematics during breaking.

One way to identify these kinematics is by measuring the water particle velocities, however this was proven to be very difficult in the past because of the lack of accurate measuring instruments to capture the velocities in the complex breaking environment characterized by air entertainment and turbulence. Nakagawa [33] mentioned in 1982 that none of the instruments available commercially, such as laser Doppler anemometers, electromagnetic flow meters, hot wires and small propellers, are suitable for such measurements. Although recently, the velocity field has been measured in laboratory experiments using the Particle Image Velocimetry (PIV) technology [10].

As a result, studying of breaking waves focused on the evolution of different parameters that can characterize the type of breaking such as wave heights and wave steepness at the breaking point [18]. Breaking conditions have been proposed theoretically using different finite amplitude wave theories to find the wave steepness and wave height at the breaking point and have been compared to laboratory experiments and breaking types have been identified based on these observations.

1.2.1 Breaking conditions

Many conditions were proposed to define when a wave breaks. Based on these conditions, analytical wave theories were used to introduce breaking limits and based on these limits, parameters such as the wave height H_b, the wave length L_b and the water depth h_b at the breaking point can be formulated.

The main conditions for breaking in the literature are:

1. Rankine [18] proposed that waves break when the wave particle velocity at the wave crest become larger than the wave celerity.

   As it is known, the water particles in the presence of a wave undergo orbital motion in shallow water (Figure 1.1). When the horizontal velocity of the par-

ticle under the wave crest increases because of shoaling and exceed the celerity of the wave itself, the waves break.

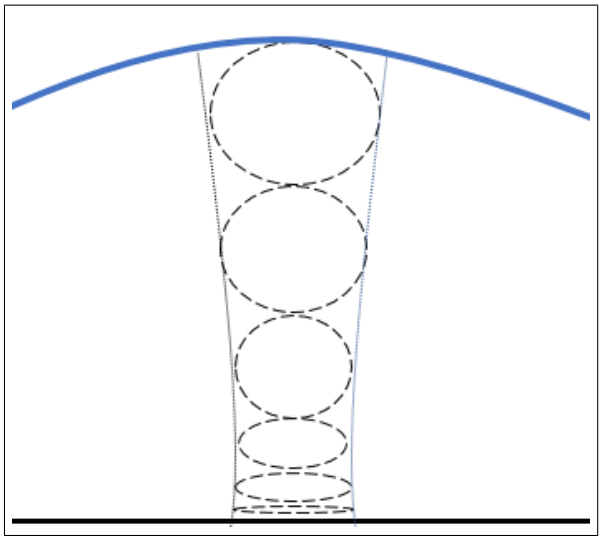

Figure 1.1: Orbital motion of water particles under the propagation of the wave in intermediate to shallow waters

Formulations have been made to translate this criterion into equations describing the wave height, wave length and water depth at the breaking point using several wave theories.

Miche (1994) has expressed the breaking limit according to Stokes wave theory to be:

$$\frac{H_b}{L_b} = 0.142 tanh(\frac{2\pi h_b}{L_b}) \tag{1.1}$$

where H_b is the wave height at breaking, L_b is the wave length at breaking, h_b is the water depth at breaking point.

Similarly, McCowan formulated an equation based on solitary wave theory and is more applicable in shallow waters:

$$\gamma = \frac{H_b}{h_b} = 0.78 \tag{1.2}$$

Where γ is the breaker index. It should be noted that these formulations correspond to waves that break on a horizontal bed. Other empirical formulas have been proposed from laboratory experiments to be used for sloping beds.

2. Stokes [18] proposed that waves break when the waves become so steep that the crest make an angle of 120° (Figure 1.2).

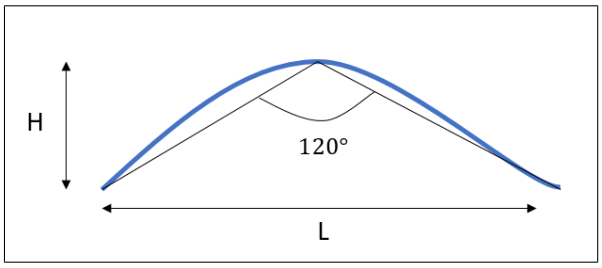

Figure 1.2: Stoke's breaking limit of 120 degree

This condition implies that waves break because of their steepness and not because of depth induced changes and usually happens in deep waters and is called white capping [8]. It should be noted that the 120° angle condition corresponds to the McCowan's criterion for the solitary wave theory.

3. When the wave structure becomes asymmetric such that the wave front surface becomes vertical.

   This condition as well was applied to wave theories describing long waves, however, the breaking point predicted by these theories depends on the initial input wave profile and this makes it harder to be applied generally [18]. Nevertheless, this condition can be useful when trying to identify wave breaking from observations of wave profile measurements or time series measurements.

1.2.2 Breaking types

In contrast to the formulations shown in the previous section, a natural seabed is not horizontal. Battjes (1974) [5] showed that the process of breaking on sloping beds takes place in various ways depending on the wave steepness and the slope of the beach according to a parameter called the Iribarren number which is given by:

$$\xi = \frac{tan\alpha}{\sqrt{H/L}} \tag{1.3}$$

Where α is the angle of the slope. The wave steepness H/L can be defined at the deep water H_0/L_0 or at the breaker point H_b/L_b these correspond to two different versions of the Iribarren number ξ_0 and ξ_b respectively.
He then classified the breaking types according to the Iribarren number based on laboratory experiments as follows:

$$\begin{cases} \text{Surging or collapsing} & \text{if} & \xi_0 > 3.3 & \text{or} & \xi_b > 2.0 \\ \text{Plunging} & \text{if} & 0.5 < \xi_0 < 3.3 & \text{or} & 0.4 < \xi_b < 2.0 \\ \text{Spilling} & \text{if} & \xi_0 < 0.5 & \text{or} & \xi_b < 0.4 \end{cases}$$

1. Spilling breakers: They are related to low Iribarren numbers and often occur along flat beaches, the waves start breaking offshore in a very gradual manner and they dissipate energy as they break so that there is very little energy reflection.

   The spilling breakers are also characterized by the white water foam layer that appears in front of the wave crest that last for a large distance.

2. Plunging breakers: this type of breakers is characterized by a lot of air entrainment as the crest curls and break over the lower part of the wave creating a lot of turbulence and as a result a secondary wave is formed and a splash usually follows. Plunging breakers will be discussed in details in section 1.2.3.

3. Surging breakers: This type of breakers are usually found along steep beaches for swell waves (low steepness waves). The waves behave like plunging breakers however before the wave crest can curl, the toe of the wave surges on the beach, thus preventing the top curling and as a result a huge percentage of the wave energy is reflected back to sea.

   Galvin [18] also defined collapsing breakers which is the transition between plunging and surging breakers. It should be noted that these values are indicative and the transition between the various breaker types is gradual.

The breaker index (γ) also depends on the breaker type. Since, the breaking processes require a certain time, waves on steeper slopes (plunging or surging) will breaker close to the shore in lower water depths which causes the breaker index $\gamma = H_b/h_b$ to increase from the typical value of 0.78 on horizontal slopes. In contrast to spilling breakers which is related to mild slopes, waves break offshore at higher water depths. Typical values of γ for plunging breakers are (0.8-1.2) and for spilling breakers (0.6-0.8) [8].

1.2.3 Wave types

As mentioned in section **??**, four cases will be simulated numerically. The incoming boundary of each of these cases is different due to the different physics. In this section, theoretical review of the types of waves proposed in each case will be given to provide the required background needed to analyze the results of the simulations.

Solitary waves

Since 1970s, the solitary wave is frequently used to model the important features of tsunamis approaching the coast [28] and it is used in case 1 (section 3.1) . A Solitary wave is a wave which propagates with a constant shape that does not change with time and have an infinite wave length theoretically. It is characterized by a wave crest with no trough (Figure 1.3). There is an agreement that a suitable physical model for

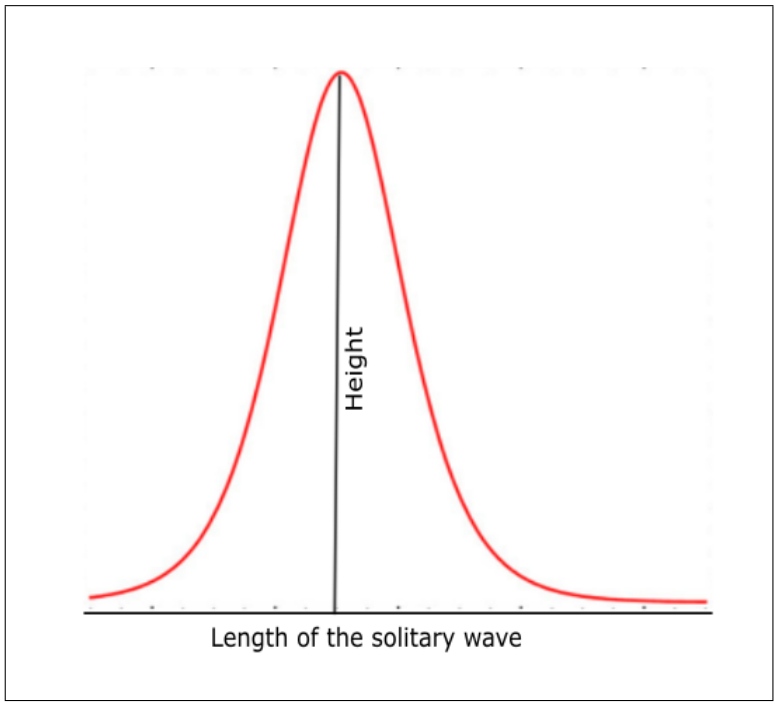

Figure 1.3: Schematic of a solitary wave with a wave crest and no wave trough

Tsunamis run-up on coasts is the formalism of a long wave propagating over constant depth and encountering a sloping beach [40]. For the propagation of long waves, the parameters: h/L & H/h are of a great importance, where L is the wave length, h the water depth and H the wave height.

h/L parameter gives an indication of the importance of frequency dispersion, when the wavelength is large compared to the water depth, the wave celerity only depends

on the water depth, the frequency dispersion can be neglected and shallow water equations can be used.

H/h parameter describes the scale of the wave height to the water depth, if $H/h << 1$ the nonlinear effects can be neglected and simplified linear shallow water equations can be adequate.

However, when the long waves approach the coast, the wave height increases and the nonlinear effects cannot be neglected anymore, that is why the full nonlinear shallow water equations should be used.

Carrier and Greenspan [9] proposed a method to solve the nonlinear shallow water equations and transform them to a set of linear equations to describe the run-up of waves on a plane slope by providing the appropriate boundary conditions. Synolakis [40] simplified the Carrier and Greenspan transformation and applied to the problem of non-breaking solitary waves propagating in a constant depth on constant slope plane beaches and generated a formulation for the maximum runup as follows:

$$\frac{R_s}{h_0} = 2.831\sqrt{cot\beta}(\frac{H}{h_0})^{5/4} \tag{1.4}$$

Where, R_s = the maximum wave run up, β = the angle of the slope, h_0 = the water depth at constant depth region, H = the incident solitary wave height at constant depth region.
In 2001, Li [25] investigated the importance of a high order correction to the solution of Synolakis as follows:

$$\frac{R}{h_0} = \frac{R_s}{h_0}(1 + \frac{R_{cr}}{R_s}) \tag{1.5}$$

$$\frac{R_{cr}}{R_s} = 0.104\ cot\beta\frac{H}{h_0} \tag{1.6}$$

Where, R_{cr}/R_s represents the nonlinear correction and R_{cr} is the difference between nonlinear and linear run up. It is found that the improvement in accuracy of the prediction of the maximum run up after the correction is of the order of 10% than the run-up from Synolakis [25].

Therefore, it can be said, that the long wave run-up according to theory is directly proportional to the incident solitary wave height and the slope of the beach and inversely proportional to the constant water depth.

Plunging breaking waves

Wave breaking is a two-phase flow processes that includes air and water interaction and involves a transition of irrotational flow into rotational flow resulting in a lot of turbulence and generation of eddies of different scales. Waves break in the near shore when the ratio of the wave height to the water depth increases to the point that the crest turnover and cause breaking of the wave.

As mentioned previously, waves can break in different ways depending on the breaker parameter ξ which is a function of the wave steepness in deep water H_0/L_0 and the slope of the beach m. Plunging breaking waves occur for values of breaker parameter ranging from 0.5 to 3.3 [11]. Plunging breaker is characterized by large air entertainment. According to Lubin, plunging breaking waves potential for air entertainment is much greater than other breaker types [27].

Pictures from Miller [31], illustrates how plunging breakers develop and affect the flow. First, the jet overturns and closes on front of the breaker to form a cavity and the wave becomes almost vertical. After that, the water body pushed up by the overturning jet creates a secondary wave [41]. This secondary wave is responsible for the generation of large scale vortex in front of the first one.The turbulence generated by these vortices along with the entrained air bubbles penetrate the entire water depth and is advected and diffused toward the bottom and as a result it significantly affect the bottom flow and causes damping of wave energy.

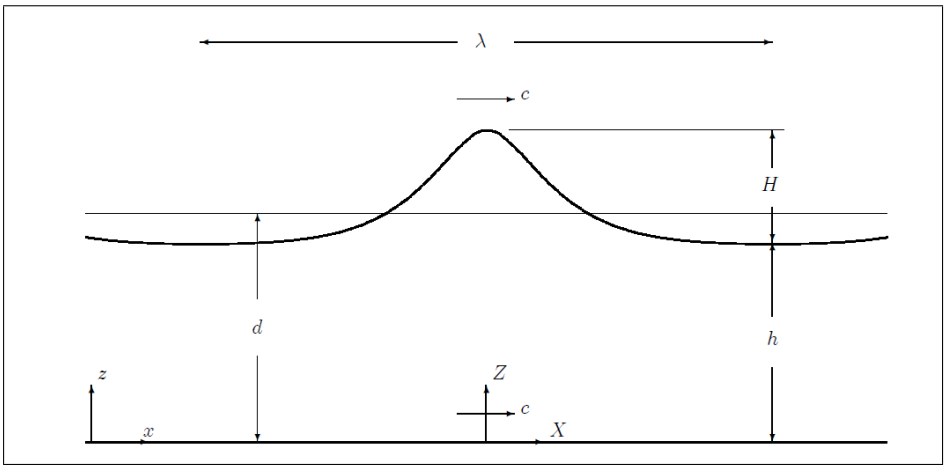

Figure 1.4: Schematic of a cnoidal wave

Because of the air entertainment and the eddies through the entire water column, the turbulent velocity varies in time through the entire water depth, in contrast to spilling breakers where the turbulent velocity only varies near the trough [26]. Therefore, the turbulence kinetic energy which is a function of the turbulent velocities is

carried upward and landward by the mean flow which is directed shorewards. That is why, waves that develop into plunging breakers tend to build up the beach because of the landward sediment transport mechanisms caused by the turbulent kinetic energy advection landwards [41].

Simulation of plunging breaking waves on a constant slope will be carried out in case 2 (section 3.2) and cnoidal waves will be imposed to represent the waves that will develop afterwards into plunging breaking waves.

Cnoidal waves are type of nonlinear periodic long waves that form a solution to the Korteweg-de Vries equation. The Korteweg-de Vries (KdV) equation describes the forward propagation of weakly nonlinear and dispersive long waves [13], for this reason this type of waves are used to model the plunging breaking waves in case 2. The name Cnoidal is a result that the wave solution is proportional to the square of the Jacobian elliptic function cn() [16].

Cnoidal waves are characterized by their narrow sharp crests and long flat troughs as seen in Figure 1.4. In the limit of infinite wavelength, the cnoidal wave will represent a solitary wave [13].

Irregular waves

The waves in the ocean behave irregularly. Irregularity means that the waves do not repeat themselves periodically in time and space but random due to the irregularity of the wind force. To define the parameters of the sea-state statistically, the water surface elevation is thought to be the sum of many harmonic components with different periods, amplitudes, phases and directions interacting with each other in a complex manner. This can be formulated according to Fourier series as follows:

$$\eta = \sum_{n=1}^{N} a_n cos(2\pi f_n t + \alpha_n) \tag{1.7}$$

where η is the free surface elevation, a_n, f_n, α_n are the amplitude, frequency and phase respectively that belong to each component. This decomposition of a wave signal is very useful in determining how the energy of the waves is distributed among the different frequencies.

The history of investigations on the mechanics of irregular wave breaking is still young [18]. This might be due to its complexity, for example a regular wave has a fixed breaking point while for irregular waves, the waves break at a boarder range and local extremas do not exist [32].

Time series analysis is used instead of spectral analysis to study the breaking process. This is done by defining individual waves in the irregular wave time series by applying a zero-crossing method and treating these individual waves similarly to a regular wave.

Zero-down crossing which bases the definition of the individual wave on the time the signal crosses the zero elevation downwards is proven to be more efficient that zero up crossing in describing waves at breaking point. This may be regarded to the fact that when waves break they generate small secondary turbulent waves and zero down crossing method is proven to be more efficient in capturing these waves [18]. After defining individual waves, breaking parameters can be investigated. Several formulas were proposed based on experimental studies and it was found that the individual waves composing the irregular wave breaks more easily (earlier) than a similar regular wave with the same properties [18].

In cases 3 and 4 (sections 3.3 and 3.4 respectively), Irregular waves will be imposed in the model to simulate their behaviour and compare it to laboratory and field measurements.

Chapter 2

Numerical model

In this chapter, the numerical model used is described. REEF3D [6] is an object oriented C++ open-source CFD model developed at the Department of Civil and Environmental Engineering at NTNU. Several complex wave hydrodynamics phenomena such as wave trapping [24], complex free surface interaction [36], wave transformation [22] [21], sediment transport [3] [4], forces due to regular and irregular waves [23] [1] and ship-induced waves [17] have previously been studied using REEF3D.

For studying the behaviour of breaking waves and capturing their evolution, accuracy play an important role. REEF3D is a CFD model which incorporates high-order discretization schemes with the level set method to obtain a sharp and accurate solution for the evolution of the free surface. Moreover, it is a two-phase model which resolves air and water which is essential in studying breaking waves as air entrainment plays an important role.

In the following sections, the equations governing REEF3D model are described, along with discretization schemes and the methods used in solving these equations. In addition, methods for capturing the free surface, wave generation and absorption in the numerical tank are presented. For more information about the model, the reader is referred to [6].

2.1 Governing equation

Navier-Stokes equations are momentum and mass conservation equations which describe the full behaviour of the flow. In REEF3D, Reynolds-Averaged Naiver-Stokes equation are used. This means that the Naiver-Stokes equations are averaged in time and a turbulence model is used to solve the closure problem resulting from the

Reynolds stress term. Turbulence modelling will be discussed extensively in section 2.2. Since REEF3D is focused on solving problems related to marine and hydraulic engineering, the flow is described as incompressible and the density can be assumed to be constant. The final form of the equations can be written as:

$$\frac{\partial u_i}{\partial x_i} = 0 \tag{2.1}$$

$$\frac{\partial u_i}{\partial t} + u_j \frac{\partial u_i}{\partial x_j} = -\frac{1}{\rho}\frac{\partial p}{\partial x_i} + \frac{\partial}{\partial x_j}(\nu(\frac{\partial u_i}{\partial x_i} + \frac{\partial u_j}{\partial x_i}) - \overline{u_i u_j}) + g_i \tag{2.2}$$

where: i and j indices refers to the three dimensions, u represents the velocity averaged over time t, x is the spatial scale, p is the pressure, g is the acceleration due to gravity and $\overline{u_i u_j}$ is the Reynolds stress.

The first equation describes the conservation of mass and since the equations are applied to incompressible flow, the final form represents that the flow is divergence free.

The second equation is the conservation of momentum in all three directions of the flow. The first term is the rate of change of velocity with respect to time. The second term is the convection term. On the right hand side of the equation contains the pressure gradient and the diffusive term which works on smoothing the gradients and is characterized by second derivatives, in addition to the Reynolds stress term which arises from the fluctuations of the turbulent velocity.

2.2 Turbulence modelling

The Reynolds averaged equations are used in REEF3D. These equations introduce the Reynolds stress term which describes the turbulent stress that causes the fluctuations in the velocity field. Boussinesq related the Reynolds stress to the velocity gradient and an eddy viscosity term which gives an indication of the amount of turbulent mixing according to the following equation:

$$-\overline{u_i u_j} = \nu_t(\frac{\partial u_j}{\partial x_i} + \frac{\partial u_i}{\partial x_j}) - \frac{2}{3}k\delta_{ij} \tag{2.3}$$

Therefore, the problem is shifted from calculating the Reynolds stress to finding the value of the eddy viscosity. This value is modelled in REEF3D using the transport

equations that describe the eddy viscosity as a function of the turbulent kinetic energy and the specific turbulent dissipation $(k-\omega)$ model.

$$\frac{\partial k}{\partial t} + u_j \frac{\partial k}{\partial x_j} = \frac{\partial}{\partial x_j}((\nu + \frac{\nu_t}{\sigma_k})\frac{\partial k}{\partial x_j}) + P_k - \beta_k K\omega \tag{2.4}$$

$$\frac{\partial \omega}{\partial t} + u_j \frac{\partial \omega}{\partial x_j} = \frac{\partial}{\partial x_j}((\nu + \frac{\nu_t}{\sigma_\omega})\frac{\partial \omega}{\partial x_j}) + \frac{\omega}{k}\alpha P_k - \beta\omega^2 \tag{2.5}$$

$$\nu_t = min(\frac{k}{\omega}, \sqrt{\frac{2}{3}}\frac{k}{\mid S \mid}) \tag{2.6}$$

where P_k is the turbulent production rate and the closure coefficients have the following values: $\sigma_k = 2$, $\sigma_w = 2$, $\alpha = 5/9$, $_k = 9/100$, $\beta = 3/40$. S is the mean strain rate, which can be large in case of oscillatory motion. The eddy viscosity is limited by the value of $\sqrt{\frac{2}{3}}\frac{k}{|S|}$ to avoid overproduction of turbulence in flow outside the boundary layer.

At the free surface however, the large density differences between air and water causes large strains at the free surface which is not physical. Hence, the dissipation at the free surface is given by [34]:

$$\omega_s = \frac{C_\mu^{-\frac{1}{4}}}{k} k^{1/2}.(\frac{1}{y'} + \frac{1}{y*}) \tag{2.7}$$

Where, $c_\mu = 0.07$ and $k = 0.4$. y' is the virtual origin of the turbulent length scale and has a value of 0.007 times the water depth. $y*$ is the distance from the nearest wall to ensure a smooth transition to the wall value of ω.

2.3 The numerical scheme

To solve the Navier-Stokes equation numerically, the continuous domain of the physical phenomena of the fluid flow needs to be discretized in space and solved for each time step until the end of the simulation time. To determine a numerical scheme for this discretization, several properties needs to be taken into account:

1. Convergence: The solution of the numerical scheme must converge to the real solution of the partial differential equation, and the way to check convergence of a numerical scheme is by checking its consistency and stability. If the numerical scheme is consistent and stable then its solution will converge to the real solution.

- Consistency: this property means that the behaviour of the numerical scheme is the same as the partial differential equation, a simple way to check that is by calculating the truncation error. A consistent scheme's truncation error will approach zero as $\Delta t \rightarrow 0$.
- Stability: stability of a numerical solution ensures that the solution stays bounded and does not diverge with time.

2. Accuracy: Means to maintain a solution that does not produce numerical damping which results in unnphysical damping of the waves. A scheme with high accuracy ensures that the numerical solution will converge to the real solution.

3. Monotonicity: ensures that the numerical scheme does not introduce numerical oscillations.

4. Efficiency: the computational model needs to be efficient and fast, and in the era of parallel computation this can be achieved.

REEF3D uses a finite difference method to solve the partial differential equations. The finite difference method replaces the continuum representation of the equations with a set of discrete equations. It is most suitable for regular grids and since REEF3D uses a Cartesian grid it is very efficient. The Cartesian grid in REEF3D is staggered. This means that the unknown variables are not located at the same grid points, instead the velocity and the pressure variables are defined at different points. This has proven to be more efficient in avoiding the odd-even decoupling between velocity and pressure which is a discretization error that can occur on collocated grids [39]. Methods for discretization in space and integration in time that are applied in REEF3D are described in the following sections.

2.4 Space discretization

The requirements mentioned in section 2.3 are satisfied by the implementation of the fifth-order Weighted Essentially Non-oscillatory Scheme (WENO) in the conservative finite-difference framework for the convection discretization of the flow velocities [20] and by the Hamilton-Jacobi version of the WENO scheme for the level set function ϕ [38] , more information about the level set function ϕ is given in section 2.7.

The convection discretization of the flow velocity $\tilde{u}$ is obtained at the cell face through simple interpolation as follows:

$$u_i \frac{\partial u_i}{\partial x_i} \approx \frac{1}{\Delta x}(\tilde{u}_{i+1/2} u_{i+1/2} - \tilde{u}_{i-1/2} u_{i-1/2}) \tag{2.8}$$

where $i + 1/2$ and $i - 1/2$ represent the cell faces, and $u_{i+1/2}$ is reconstructed with WENO scheme based on the weighted sum of the three ENO stencils:

$$U^{\pm}_{i+1/2} = \omega^{\pm}_1 U^{1\pm}_{i+1/2} + \omega^{\pm}_2 U^{2\pm}_{i+1/2} + \omega^{\pm}_3 U^{3\pm}_{i+1/2} \tag{2.9}$$

The $\pm$ sign indicates the upwind direction. U^1 , U^2 and U^3 represent the three possible ENO stencils. For upwind direction in the positive i direction, they are:

$$\begin{aligned} U^{1-}_{i+1/2} &= \frac{1}{3}u_{i-2} - \frac{7}{6}u_{i-1} + \frac{11}{6}u_i \\ U^{2-}_{i+1/2} &= -\frac{1}{6}u_{i-1} + \frac{5}{6}u_i + \frac{1}{3}u_{i+1} \\ U^{3-}_{i+1/2} &= \frac{1}{3}u_i + \frac{5}{6}u_{i+1} - \frac{1}{6}u_{i+2} \end{aligned} \tag{2.10}$$

The nonlinear weights $\omega^{\pm}_n$ are determined for each ENO stencil and calculated based on smoothness indicators IS [20] . The WENO scheme can handle large gradients right up to the shock very accurately, In the worst case the accuracy will be of the third order. However, for a smooth solution, the WENO scheme delivers fifth order accuracy. In addition to that, the scheme does not smear out gradients and maintain its sharpness and is conservative.

2.5 Time integration

For the time stepping in REEF3D, the momentum equations and the level set equation are treated differently than the turbulence model equations.
The total variance diminishing TVD Runge-Kutta scheme is used for the momentum equations, level set function and all the transport equations except the turbulence model equations. Example of TVD scheme for the level set function:

$$\begin{aligned} \phi^{(1)} &= \phi^n + \Delta t L(\phi^n) \\ \phi^{(2)} &= \frac{3}{4}\phi^n + \frac{1}{4}\phi^{(1)} + \frac{1}{4}\Delta t L(\phi^{(1)}) \\ \phi^{n+1} &= \frac{1}{3}\phi^n + \frac{2}{3}\phi^{(2)} + \frac{2}{3}\Delta t L(\phi^{(2)}) \end{aligned} \tag{2.11}$$

This explicit scheme provides a third-order temporal accuracy and if the CFL number is below 1, it shows very good numerical stability, the time step restriction is thus represented by:

$$\Delta t \leq 2\Bigg((\frac{\mid u \mid_{max}}{dx} + D) + \sqrt{(\frac{\mid u \mid_{max}}{dx} + D)^2 + \frac{4 \mid S_{max} \mid}{dx}}\Bigg)^{-1} \tag{2.12}$$

With the contribution from the diffusion term D:

$$D = max(\nu + \nu_t).\Big(\frac{2}{(dx)^2} + \frac{2}{(dy)^2} + \frac{2}{(dz)^2}\Big) \tag{2.13}$$

In a RANS model, the magnitude of turbulence expressed through the value of the eddy viscosity can be large and the condition for the diffusion part can be prohibitively restrictive and thus D is taken implicitly.

For the turbulence model transport equation $(K-\omega)$, the production and dissipation terms plays a more important role than diffusion and convection, and large source terms (production and dissipation) result in significantly smaller time steps due to the CFL criterion. For this reason, the turbulence equations are discretized using the implicit Euler method.

2.6 Solving the Navier-Stokes equation

After space and time discretization of the Navier-stokes equation, the non-hydrostatic pressure term must be obtained to fully provide a complete scheme for a numerical solution. However, a direct solution is not possible due to the involvement of non-linear terms which make the solution computationally very expensive.
The most common method to solve the pressure problem is by using the Chorin's projection method [12]. The idea behind this method is limiting the flow field to be divergent free. The first step is solving the momentum equation without the pressure gradient for an intermediate velocity field u_i^*:

$$\frac{\partial u_i^*}{\partial t} + u_j^n \frac{\partial u_i^n}{\partial x_j} = \frac{\partial}{\partial x_j}\Big[(\nu + \nu_t)\Big(\frac{\partial u_i^n}{\partial x_j} + \frac{\partial u_j^n}{\partial x_i}\Big)\Big] + g_i \tag{2.14}$$

However this intermediate velocity will not be divergent free ($\frac{\partial u_i^*}{\partial x_i} \neq 0$), but will be used to solve the pressure limiting equation for the creation of a divergent free flow field:

$$\frac{\partial}{\partial x_i}\Big(\frac{1}{\rho(\phi^n)}\frac{\partial p^{n+1}}{\partial x_i}\Big) = \frac{1}{\Delta t}\frac{\partial u_i^*}{\partial x_i} \tag{2.15}$$

Equation 2.15 is a Poisson pressure equation which is very hard to solve because it involves a linear system of equation and the coefficients of the matrix are anisotropic

and is very computationally demanding. In REEF3D, the Poisson pressure equation is solved using the iterative BiCGStab algorithm from the HYPRE solver library which contains high performance preconditioners for solutions of large and sparse linear systems on parallel computers [15]. This method ensures a fast and scalable solution to the Poisson equation. After the pressure value is known for the new time step, the intermediate velocity can be corrected to be divergent free according to the following equation:

$$u_i^{n+1} = u_i^* - \frac{\Delta t}{\rho(\phi^n)} \frac{\partial p^{n+1}}{\partial x_i} \tag{2.16}$$

2.7 Free surface

As mentioned before, REEF3D is a two-phase model, resolving air and water. In many applications, including breaking waves, the interface between these phases is a moving interface and several factors increase the difficulty of capturing this free surface, these factors include surface tension effects, density ratios, temperature jumps across the interface. REEF3D uses the level set method [37] to capture the free surface on a fixed Eulerian mesh. The level set function gives the closest distance to the interface Γ by assigning different signs for each phase acorrding to the following formulation :

$$\phi(\overrightarrow{x}, t) \begin{cases} > 0 \text{ if } & \overrightarrow{x} \in phase1 \\ = 0 \text{ if } & \overrightarrow{x} \in \Gamma \\ < 0 \text{ if } & \overrightarrow{x} \in phase2 \end{cases}$$

When the interfaces evolves and the level set function is transported by the flow, it can become distorted, so in order to avoid losing of the signed distance property and to ensure mass conservation, the level set function, re initialization of the set function is required based on the following scheme [26]:

$$\frac{\partial \phi}{\partial t} + S(\phi)\big(\mid \frac{\partial \phi}{\partial x_j} \mid -1\big) = 0 \tag{2.17}$$

2.8 Wave generation and absorption

Boundary conditions are an essential part of any numerical model and can significantly affect its results. In REEF3D, several wave theories are implemented, for example [6]: linear waves, 2nd-order and 5th order Stokes waves, 1st-order and 5th-order cnoidal waves, 1st-order and 5th order solitary waves, first-order irregular and focused waves and wave reconstruction method for irregular waves (section 2.8.3). These

wave theories can be imposed in REEF3D mainly with two methods: Dirichlet and Relaxation method.

2.8.1 Dirichlet method

Dirichlet method works by imposing a fixed value of velocity (horizontal and vertical) for each time step at the wave generation boundary. This method is the simplest, fastest and the first to be used in most models. However, since the free surface is in constant motion and the flow direction changes periodically the Dirichlet type does not always deliver waves of the highest quality [6].

2.8.2 Relaxation method

The relaxation method [14] [30] is implemented in REEF3D and works by ramping the values for the velocities and free surface from the computational values to the values obtained from the wave theory. This process of ramping will prevent any disturbances occurring in the model because of the incoming conditions and the relaxation zone distance is typically of one wave length.

Similarly, at the end boundary the waves are dissipated in the same manner to avoid reflections that can negatively affect the results. The computational values for the horizontal and vertical velocities are reduced to zero gradually, the free surface is reduced to the still water level and the pressure is reduced to the hydrostatic distribution for the still water level. The numerical beach zone which works on gradually decreasing the values to their still conditions is typically of two wave lengths [19].

2.8.3 Wave reconstruction method

In laboratory or field experiments, Irregular waves are generated based on specific spectral parameters (H_s, T_p), to simulate a numerical model of the experiment, these spectral parameters can be input in the model to generate an energy spectrum which is similar to the energy spectrum of the experiment. This will allow for a comparison of the evolution of the energy spectra of the numerical and experimental over distance and time, However a comparison of surface elevation time series for example is not possible because the waves generated will be random.

The idea of wave reconstruction method which is applied in cases 3 and 4 (Sections 3.3 and 3.4 respectively) is to use a measured time series of the surface elevation in the offshore boundary (usually in front of the wave board in laboratory experiments) and decompose this time series into its Fourier components so the phase, frequency and amplitude information is known, to be able to generate the exact similar waves in the numerical tank. This method enables the comparison of free surface numerical and experimental time series.

Using the Fast Fourier Transformation (FFT) the time series of the free surface near the wave board can be described as the summation of the Fourier components according to:

$$\eta(t) = \sum_{k=1}^{N} C_k e^{ik\omega t}$$

Next, the computed wave amplitude A_k, angular frequency ω_k and phase angles ϵ_k are given as input to the numerical model, more information about this method can be found in [2].

Chapter 3

Results

This chapter presents the results of the numerical simulations performed with REEF3D. Comparison with experimental measurements is done for all the four cases and observations are discussed.

3.1 Case 1: Solitary wave runup

Tsunamis are long water waves of small steepness that are generated by large undersea earthquakes at tectonic plate boundaries. When the tectonic plates rise or fall due to an earthquake, it displaces the water column above it and launches the rolling waves that will become a tsunami. These long waves increase in height significantly as they approach the shore as a result of shoaling and can reach heights of over 30.5 meters and can travel as fast as 805 Km/hr [42].

The run-up of these tsunami waves at the shoreline can be very destructive and can cause severe damage.Therefore, it is important to study these catastrophic waves to simulate them and think of mitigation or protection plans for their effects.

In the first case, a solitary wave which represents a tsunami wave is modelled on a plane slope and run up is compared to the experimental results. This will work as a first step towards understanding the behaviour of the waves as they approach the coast.

3.1.1 Experimental set-up

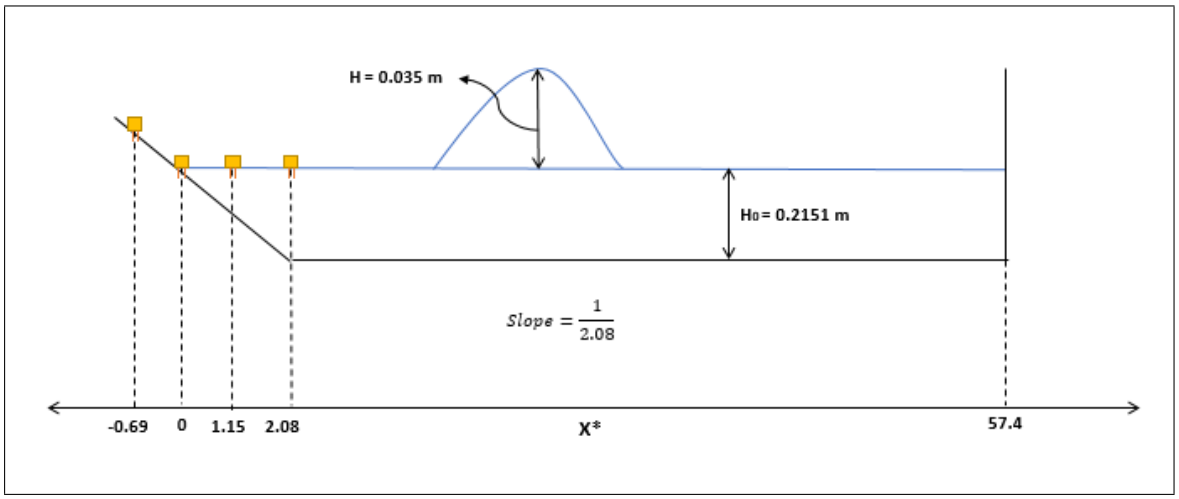

Figure 3.1: Solitary wave run-up experimental set-up: x*=0 starts at the intersection between the still waterline and the slope, the start of the slope is located at x*=2.08 according to the experiment.

The experiment on solitary wave run-up on plane slopes is performed by Li and Raichlen [25]. It was performed in a wave tank 15.25 m long, 39.6 m wide and 0.61 m deep. The water depth is kept at 0.2151 m. A plane slope of 1/2.08 is constructed from anodized aluminum plate and is 12.35 m away from the wave generator. The experimental set-up is shown in figure 3.1. $X^* = 0$ refers to the location of the original shoreline and values offshore are positive, values onshore of that position, the toe of the slope is at $X^* = 2.08$. The slope was chosen to be steep enough so that the wave does not break during run up or run down. A wave of height of 0.035 m is generated with the programmable vertical bulkhead generator driven by a hydraulic cylinder.

The water surface time series was measured at certain locations offshore of the slope and on the slope using calibrated wave gauges. Moreover, the spatial wave profiles during the experiment was captured using a high speed Redlake video camera with a resolution of 480 x 420. The run up on the slope was measured using a run up gauge which consists of laser and a camera.

The results of the experiments are described in term of the dimensionless parameters:

$$x* = \frac{x}{h_0},\ h* = \frac{h}{h_0},\ \eta* = \frac{\eta}{h_0},\ t* = t\sqrt{g/h_0} \text{ and } u* = \frac{u}{\sqrt{gh_0}}$$

3.1.2 Numerical set-up

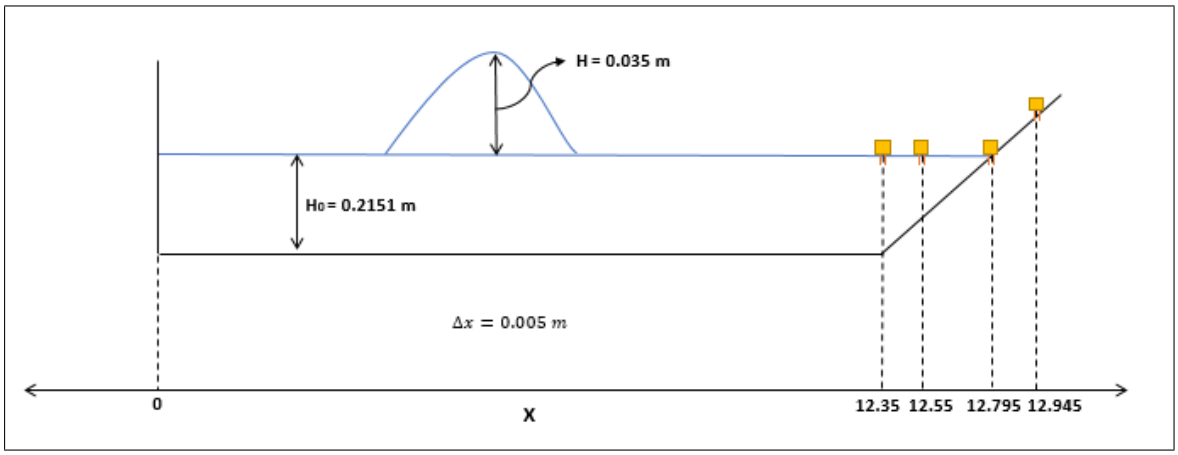

Figure 3.2: Solitary wave run-up numerical set-up: grid size = 0.005 m, four numerical wave gauges are installed along the slope to compare free surface time series

A 2D simulation is chosen for this case, since there are no changes in the bottom in the longitudinal direction. The numerical wave tank is constructed with length and height of 18 m and 1.5 m respectively. A grid size of 0.005 m is chosen for a good capturing of the run up process (Figure 3.2). In the figure, the wave gauge locations are also shown. They correspond to $x* = 2.08,\ 1.15,\ 0$ and -0.69 in the experiment.

At the left boundary, a third-order solitary wave is used to model the tsunami wave by imposing a Dirichlet boundary condition. Dirichlet boundary condition assigns appropriate values for the free surface and the velocity in the inflow boundary only, in this case, a third order solitary wave with amplitude of 0.035 m. At the right boundary, an active absorption beach is imposed, this generates a wave opposite of the reflected wave, thus cancelling it out to ensure that the simulation results will not be affected by any reflection.

3.1.3 Results

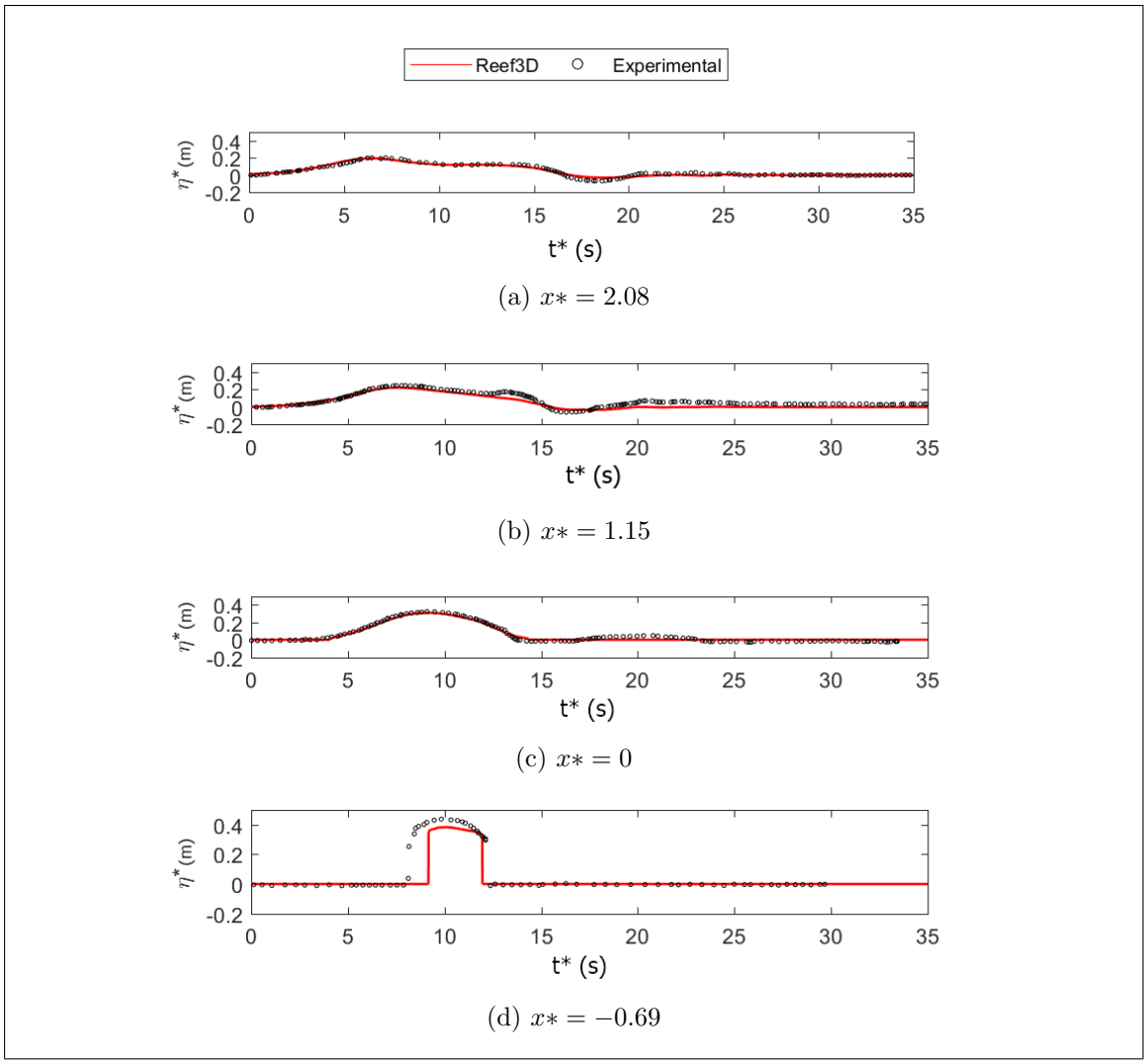

(a) $x* = 2.08$

(b) $x* = 1.15$

(c) $x* = 0$

(d) $x* = -0.69$

Figure 3.3: Time series of free surface elevation for solitary wave run-up at four locations along the slope

Time series of the dimensionless amplitudes of the free surface are shown in Figure 3.3 for the four wave gauges in the wave tank. REEF3D gives almost identical results to the experimental data. In Figure 3.3d ($x* = -0.69$), which is onshore from the position of the original shoreline, it is noticed that the increase in the values of $\eta*$ happen in the numerical simulation few seconds later than in the experiment.This may be interpreted because of the difference in the wave generation mechanisms of the experiment and REEF3D which causes this lag, however, the amplitudes are matching.

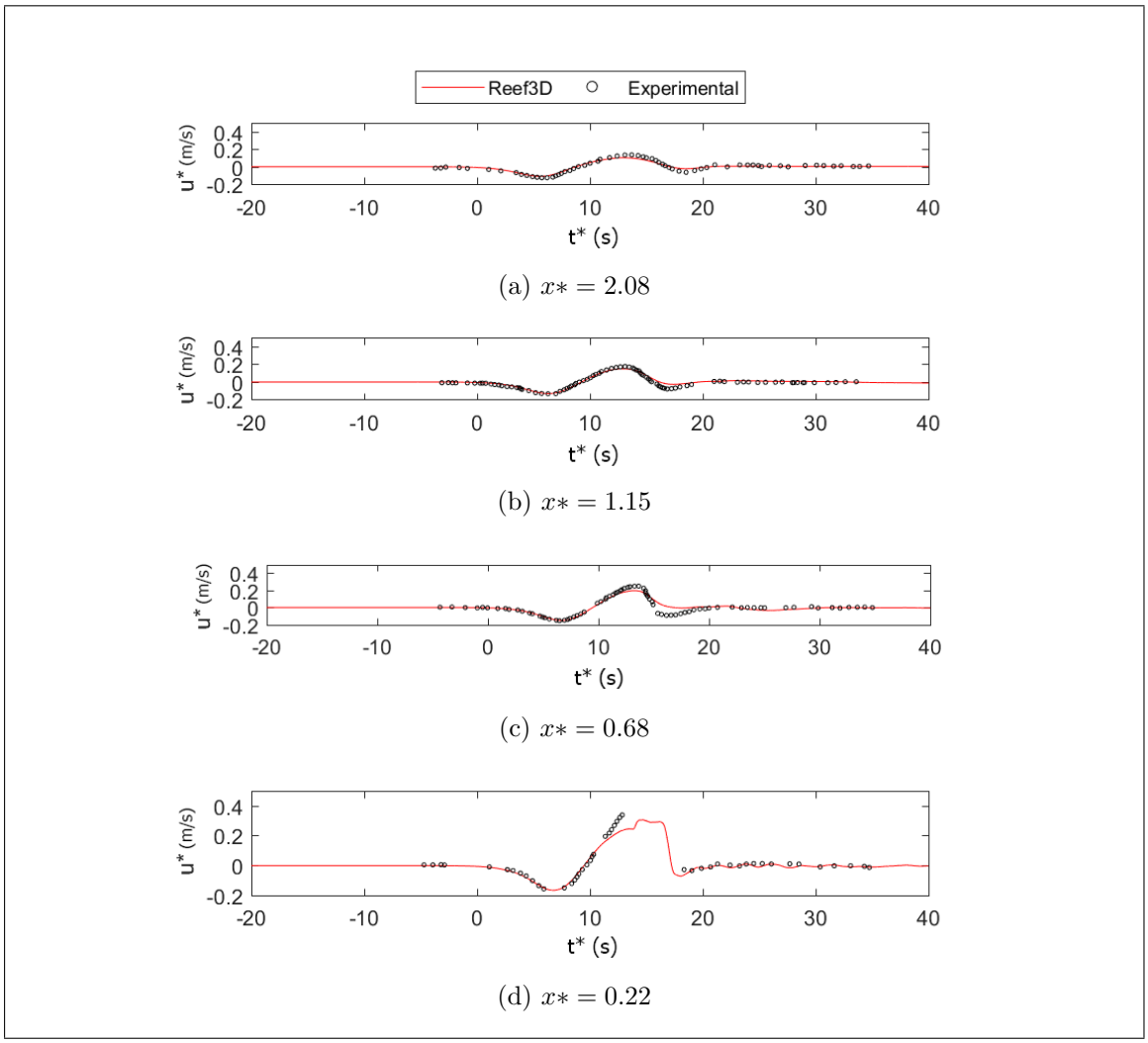

Figure 3.4: Time series of horizontal velocity for solitary wave run-up at four different locations along the slope

Figures 3.4 and 3.5 shows the horizontal and vertical velocities respectively at the locations of the velocity probes in the experiment. The velocity probes were located at mid depth of each location.

It is noticed that the horizontal velocities increase as the wave arrives and there is a very good match between numerical and experimental results. However, for the vertical velocity (w), values of the velocities are almost constant with a zero value. This can be explained from the fact that the probes are placed in the middle of the water depth where the vertical velocities are not so much affected by the incoming waves.

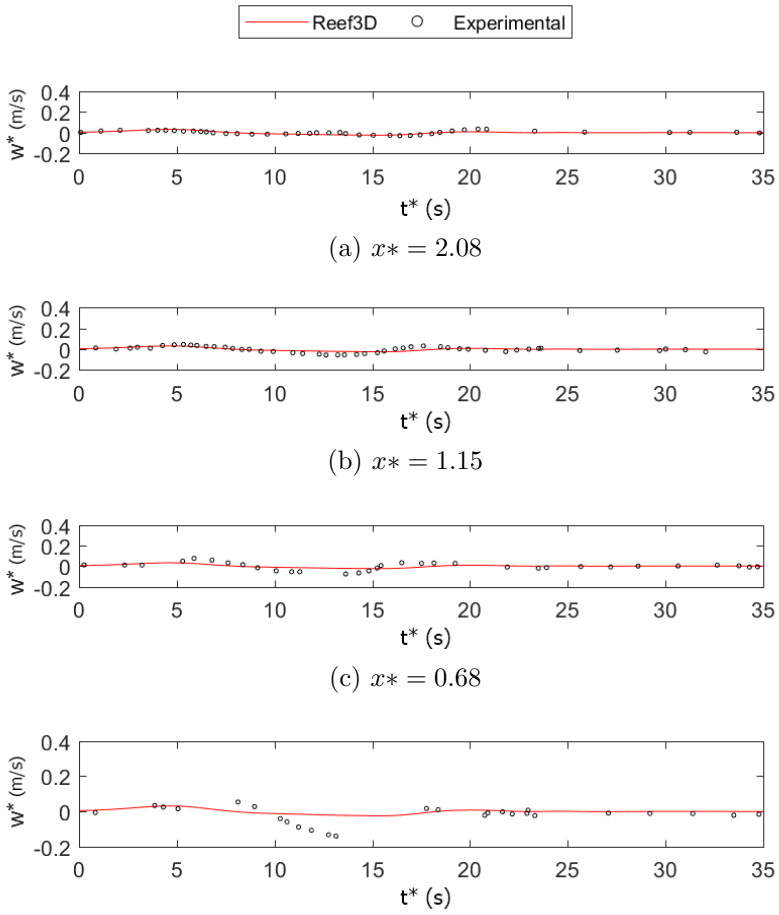

(a) $x* = 2.08$

(b) $x* = 1.15$

(c) $x* = 0.68$

(d) $x* = 0.22$

Figure 3.5: Time series of vertical velocity for solitary wave run-up at four different locations along the slope

In addition to the wave amplitude and velocities time series, a spatial view was obtained from the numerical model to investigate the run-up more closely. In Fig. 3.6, the experimental data is shown as black dots and is compared to REEF3D at different dimensionless times. There is a very good agreement between the two results specially at $t* = 8.2$, 10, 2 and 12.2 during the run-up. However, during the rundown there is a slight mismatch which is not significant.

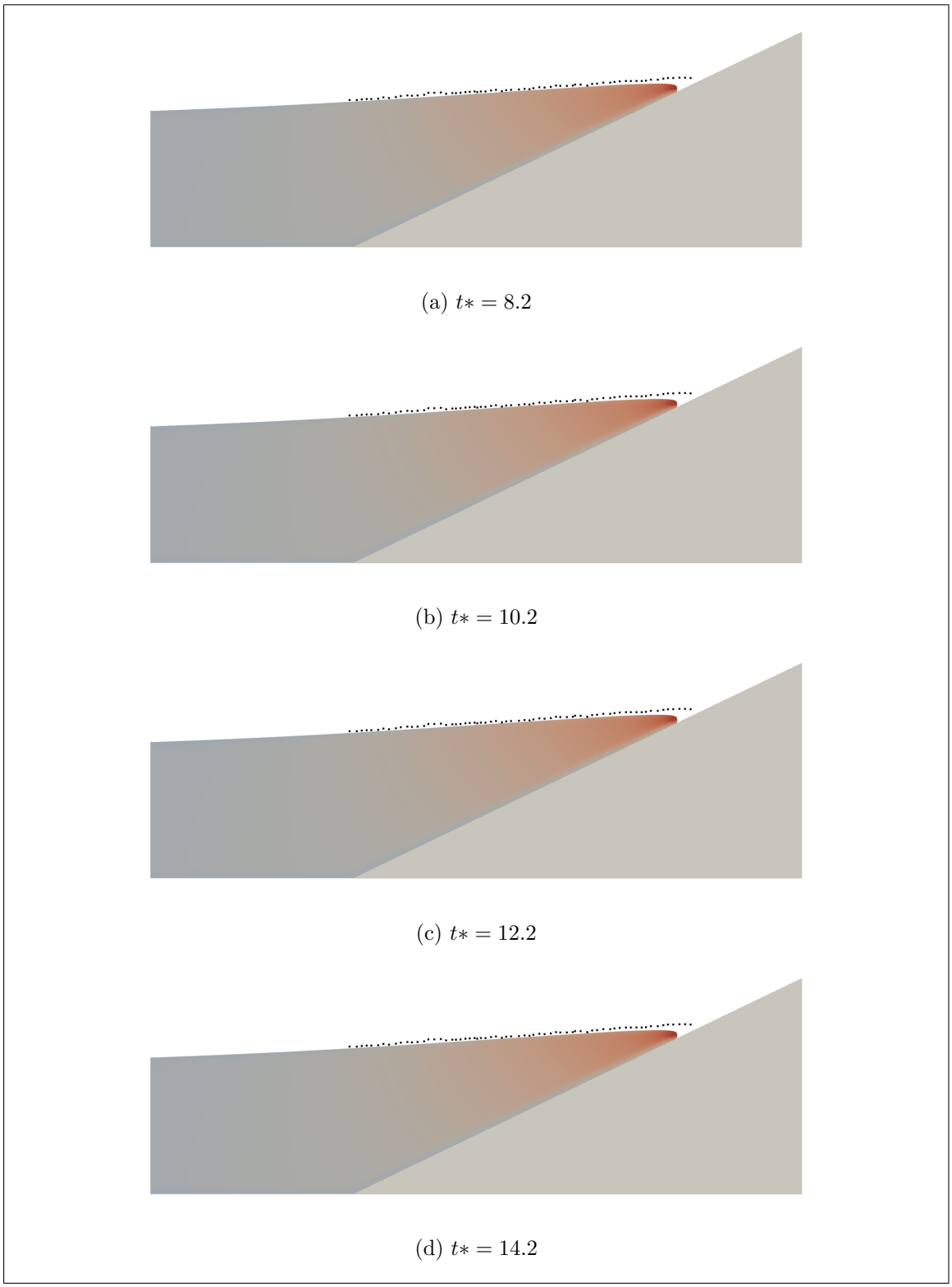

(a) $t* = 8.2$

(b) $t* = 10.2$

(c) $t* = 12.2$

(d) $t* = 14.2$

Figure 3.6: Numerical and experimental run-up comparison at four different experimental times ($t*$)

3.2 Case 2: Plunging breaking waves on a constant slope

Studying plunging breaking waves is important because these type of waves result in a large amount of energy dissipation and cause large onshore currents which result in sediment transport. In this section, the experiments by Ting and Kirby [41] plunging breaking waves on constant plane beaches are simulated in REEF3D. This is another step towards validating the model for simulating breaking waves and understanding wave transformations in the near shore region.

3.2.1 Experimental set-up

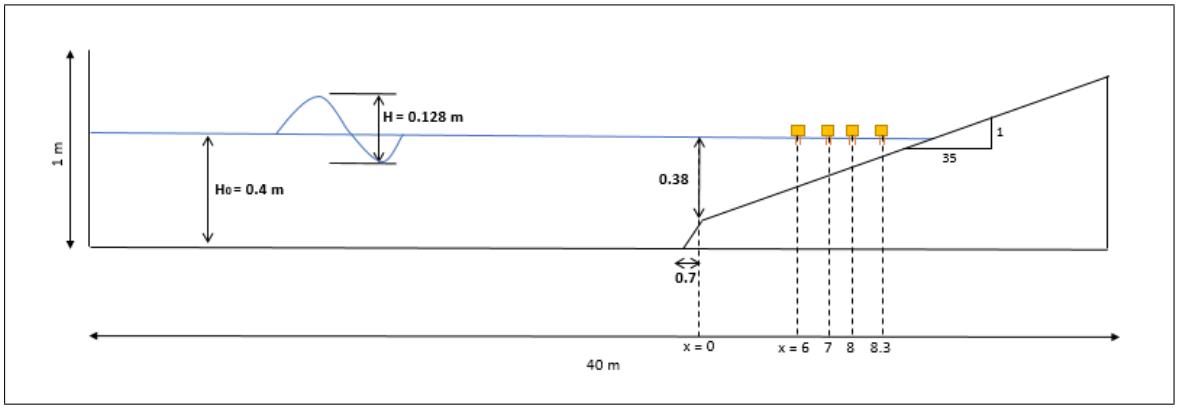

Figure 3.7: Experimental setup for Ting and Kirby [41]: $x = 0$ represents the start of the slope ($m = 1 : 35$

The wave tank is 40 m long, 0.6 m wide and 1.0 m deep. A uniform mild slope of $1 : 35$ is installed using plywood and a cnoidal wave with a height of 0.128 m in the constant depth region and a wave period of 5.0 seconds is generated from a bulkhead wave generator. The experimental setup is shown in Figure 3.7 and shows the still waterlevel of 0.4 m through the entire tank.

According to this setup, the wave steepness in deep water is 0.00328 which makes the Iribarren number $\xi = 0.5$ and the wave can be classified as a plunging breaker. Free surface elevations are measured at several locations after the slope using a capacitance wave gauge. Moreover, horizontal and vertical velocities were measured using Laser Doppler anemometer (LDA). The inaccuracies in the velocity measurement because of the LDA is estimated to be around 0.5 cm/sec.

The data is taken from the measurement devices after at least 20 minutes to ensure that the measurements are not affected by the initial conditions and they correspond to the steady state condition in the wave tank. It is important to note as well that because of the large entrainment of air in the plunging breakers it is very difficult to obtain velocity measurements with the LDA [26]. That is why during the experiment, signal drop out was noticed when the air blocked the laser beams of the LDA. As a result, some velocity signals were not taken into account in the data analysis.

3.2.2 Numerical set-up

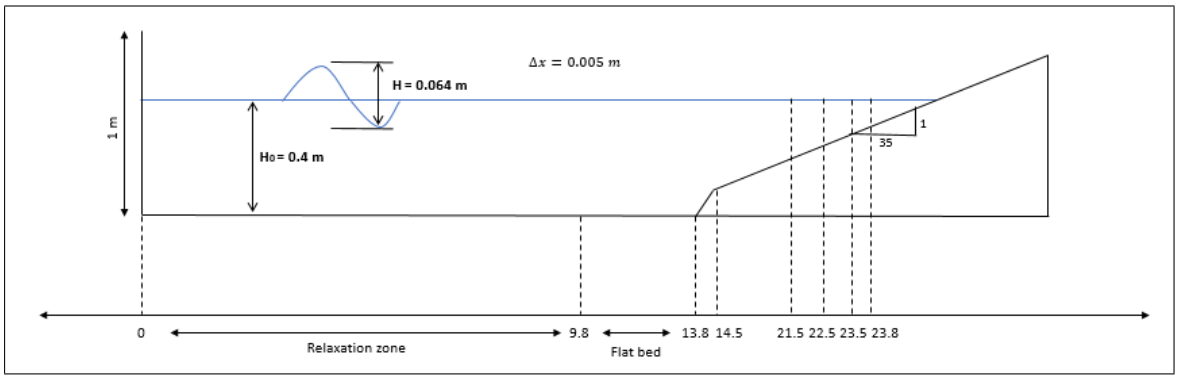

Figure 3.8: Numerical setup for plunging breaking waves: grid size = 0.005 m, the first 9.8 m represent a relaxation zone for wave generation and is equal to one wave length, followed by 4 m flat bed

Figure 3.8 shows the numerical set-up used in the simulation. First there 9.8 m the value of one wave length which is required for the relaxation method to generate the 5th-order cnoidal waves, followed by a 4m flat bed.

The slope starts 13.8 m from the beginning of the wave tank. The right boundary is at a distance of 40 m from the left boundary where a numerical beach is used to dissipate the wave energy and bring free surface to the still water level. The simulation is excuted in 2D because there are no gradients in the transverse Y direction and a gird of 0.005 m was chosen to allow for better capturing of the behaviour of breaking. The left boundary is the incoming wave boundary where the relaxation method is used to generate fifth-order cnoidal waves.

3.2.3 Results

Using REEF3D, the simulation is carried out and results for the surface elevation η, horizontal and vertical velocities were obtained.From the comparison of the numerical and experimental data, the numerical data from the third wave onward are used. This is done to ensure that the numerical results correspond to the steady state situation without effects from the wave generation in still water.

Fig. 3.9 shows the time series of the free surface elevation at different locations. There is a good match between the numerical and experimental results. More results for several other locations are shown in Figs. 3.13, 3.14, 3.15, 3.16, 3.17.

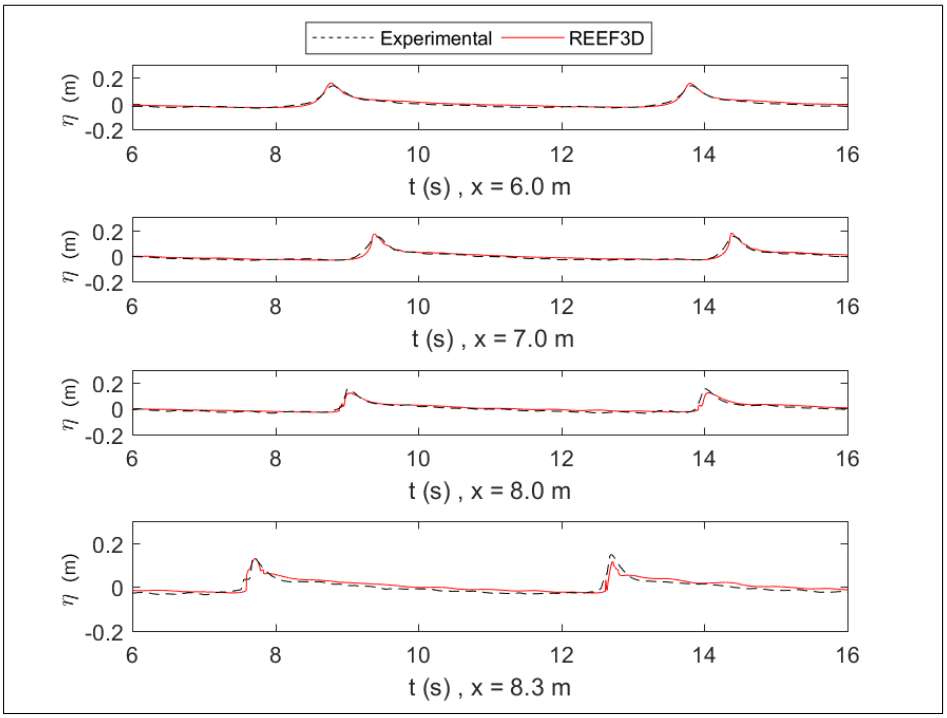

Figure 3.9: Free surface elevation time series comparison at the main four locations described in the experiment

The results of the simulation also include the horizontal and vertical velocity u and w.
In Fig. 3.10, time series of the horizontal velocity are shown at three different locations: $x = 7.295$ m a point before breaking of the wave, $x = 7.725$ m a point at the location of breaking, $x = 8.345$ m a location after breaking. In each of these locations the velocity were measured at two different heights along the water column (z=0 correspond to the still water level).

The increase in the horizontal velocity is noticed during breaking and then it reduces after breaking. Moreover, the deviation of the numerical results from the experimental results increases after breaking due to the complex processes of mixing and turbulence.

For the vertical velocities (Fig 3.11), the numerical results are slightly higher than the experimental. This can be a result of an experimental error because of the difficulties in capturing the velocities with the LDV or can be a result of a numerical error because of the air phase parameters and the damping of turbulence mechanisms in the mixing layer between the two phases.

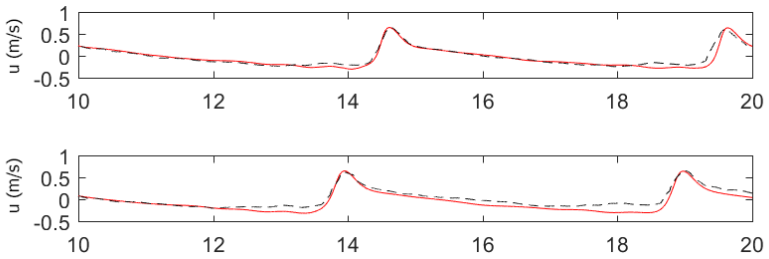

(a) horizontal velocity time series comparison at $x = 7.295m$ (before breaking): Top z= - 0.05 m, bottom z= -0.15 m, where z=0 represents the still water level

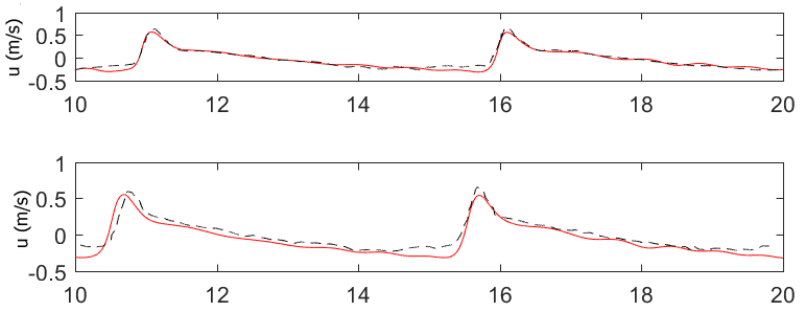

(b) horizontal velocity time series comparison at $x = 7.725m$ (during breaking): Top z= - 0.05 m, bottom z= -0.14 m, where z=0 represents the still water level

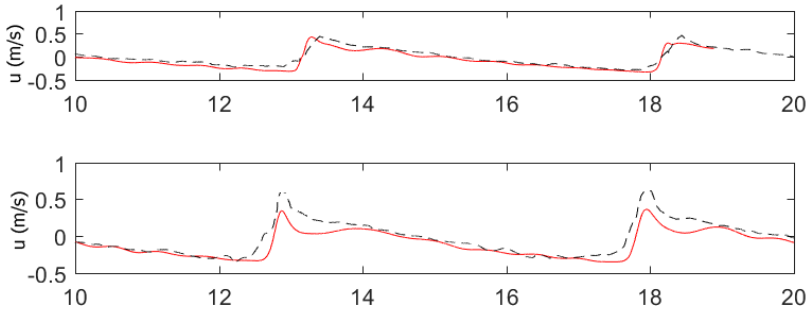

(c) horizontal velocity time series comparison at $x = 8.345m$ (after breaking): Top z= - 0.05 m, bottom z= -0.12 m, where z=0 represents the still water level

Figure 3.10: Horizontal velocity time series comparison: REEF3D (red), experimental (black)

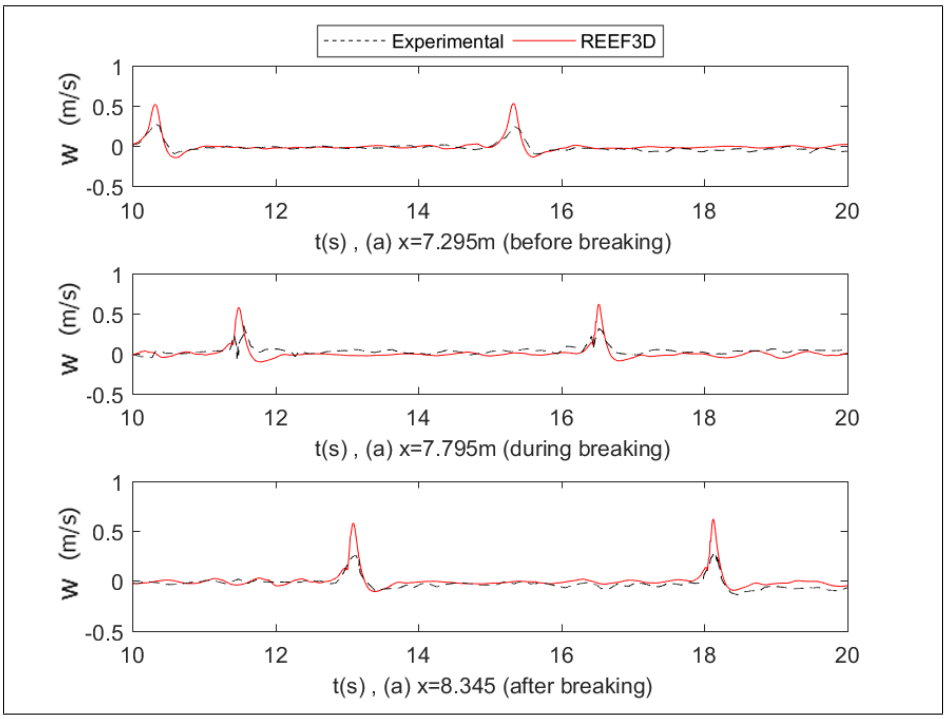

Figure 3.11: Vertical velocity time series comparison: REEF3D (red), experimental (black)

In addition to time series data, a spatial snapshot can be obtained from REEF3D which shows the plunging breaker evolution through time (Figure 3.12). In a) the crest starts to curl and the jet is about to overturn, b) the jet overturns and hits the water body. c) a secondary wave is created, which overturns as well. d) a third wave is formed and the air is entrainment is advected to the bottom.This is totally comparable with Miller illustrations [31]. It is also noticed the decay in energy which can be seen from the decrease in the magnitude of the horizontal velocity as the wave break.

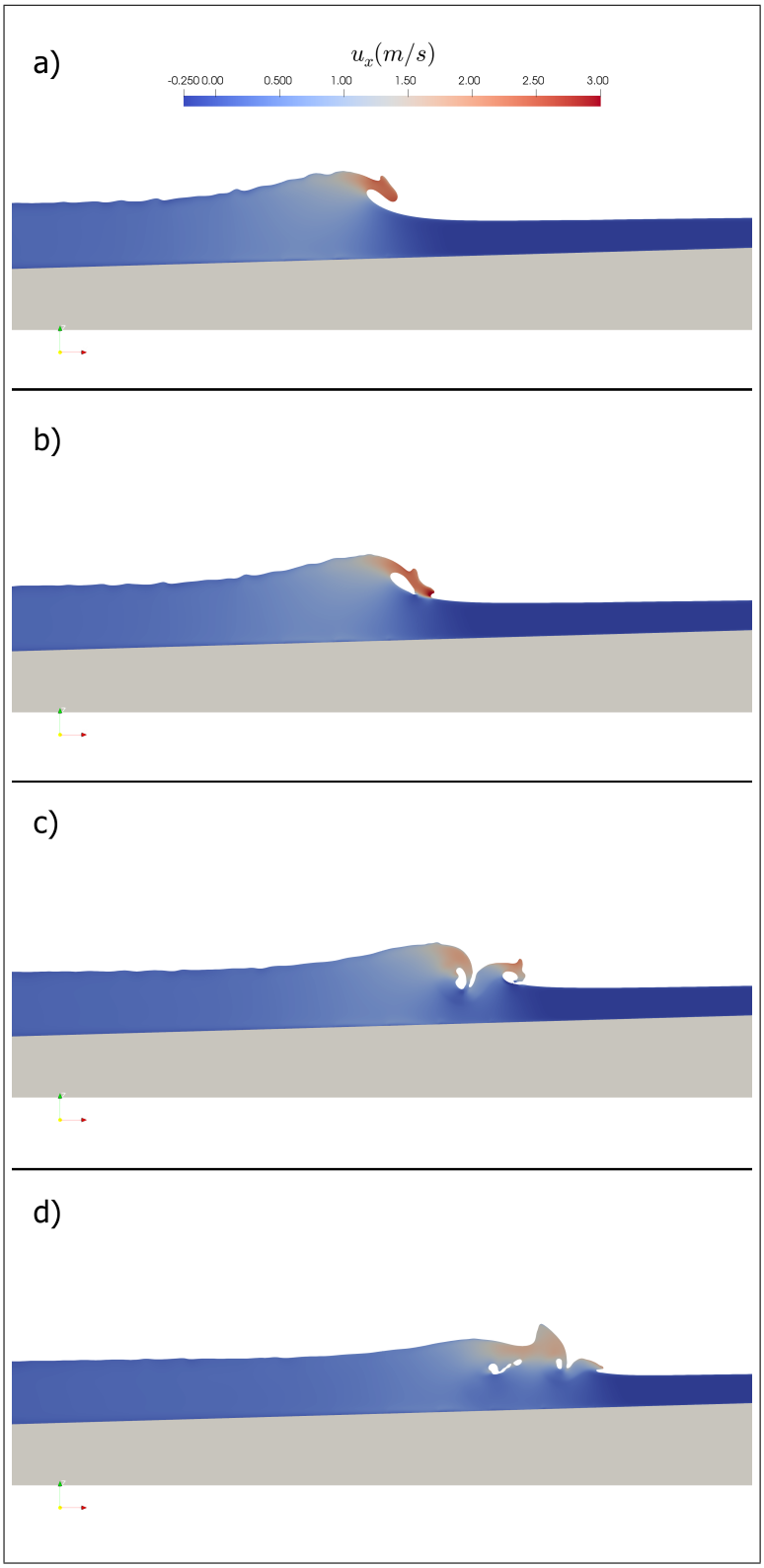

Figure 3.12: Spatial view of the plunging breaking using REEF3D at four different times: a) t= 8.04 s, b) t= 8.06 s, c) t= 8.12 s, d) t= 8.16 s

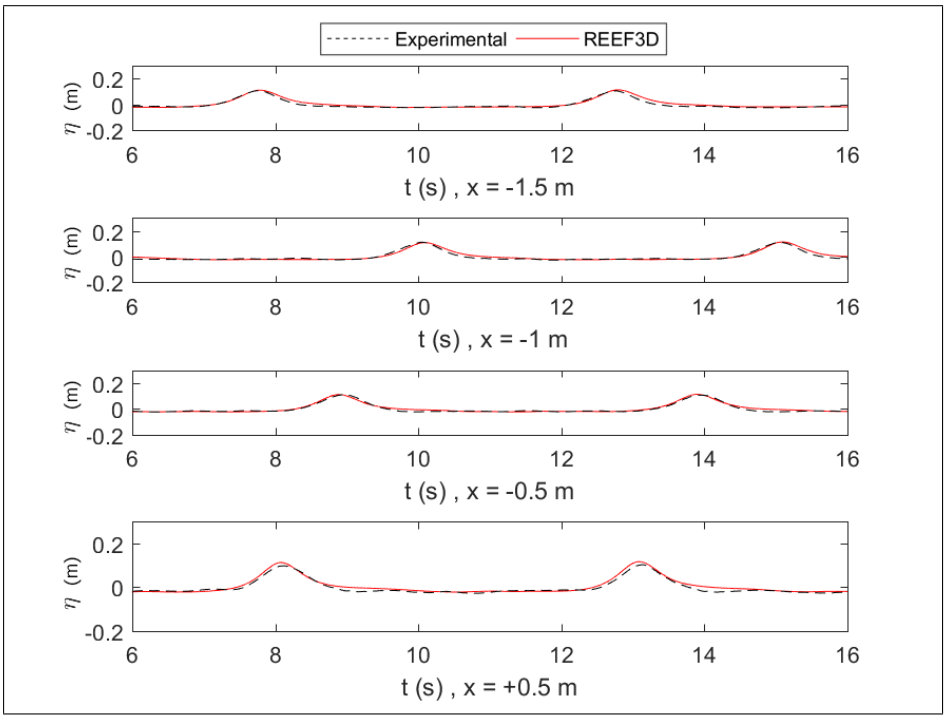

Figure 3.13: Free surface elevation time series comparison at four locations, ($x = 0$) represents the start of the slope

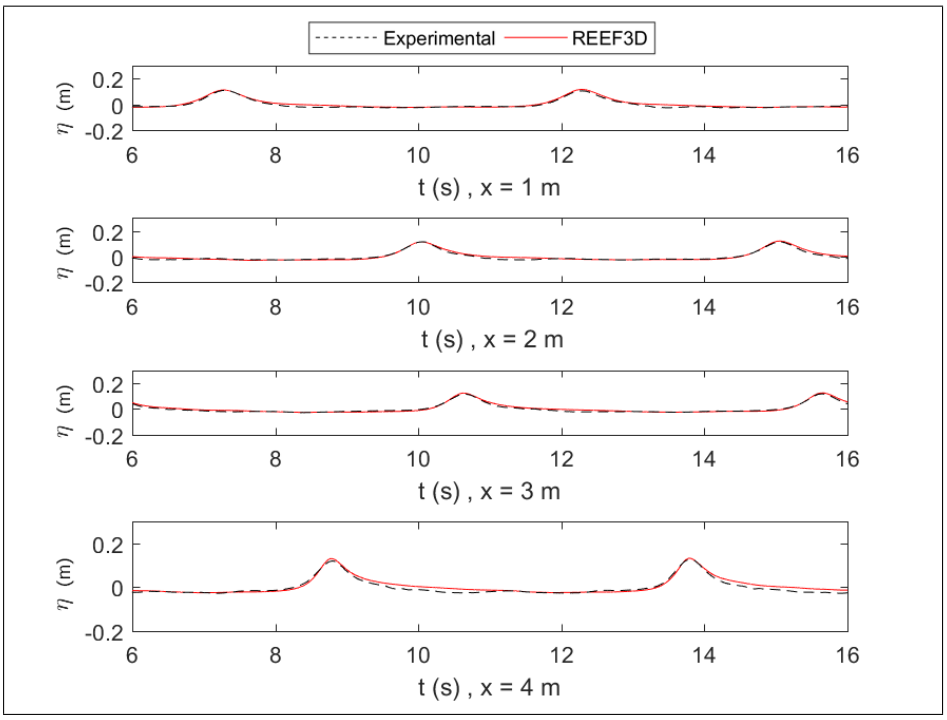

Figure 3.14: Free surface elevation time series comparison at four locations, ($x = 0$) represents the start of the slope

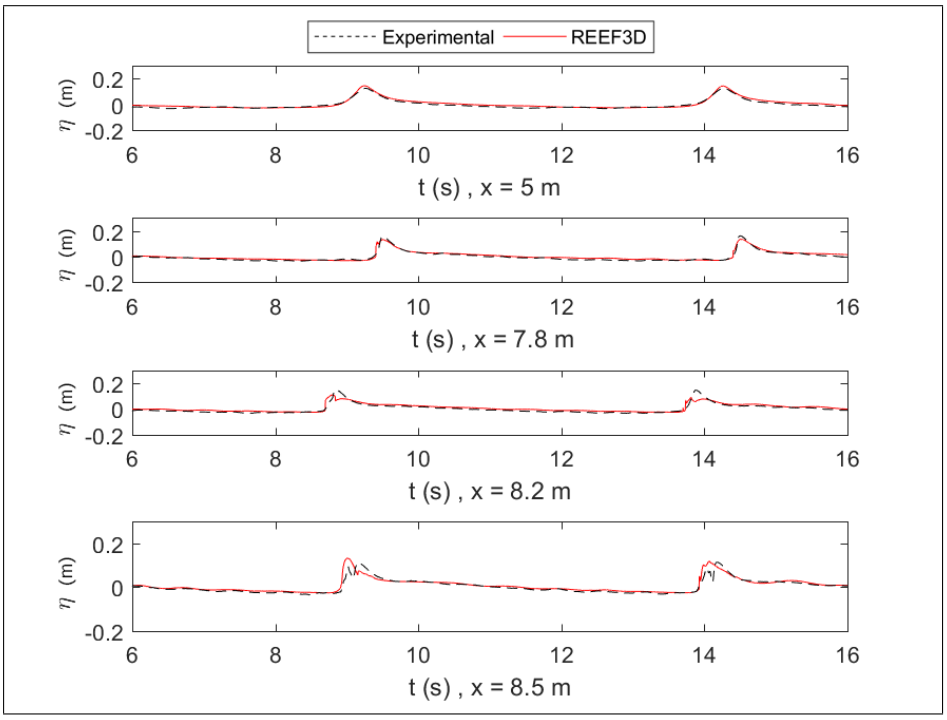

Figure 3.15: Free surface elevation time series comparison at four locations, ($x = 0$) represents the start of the slope

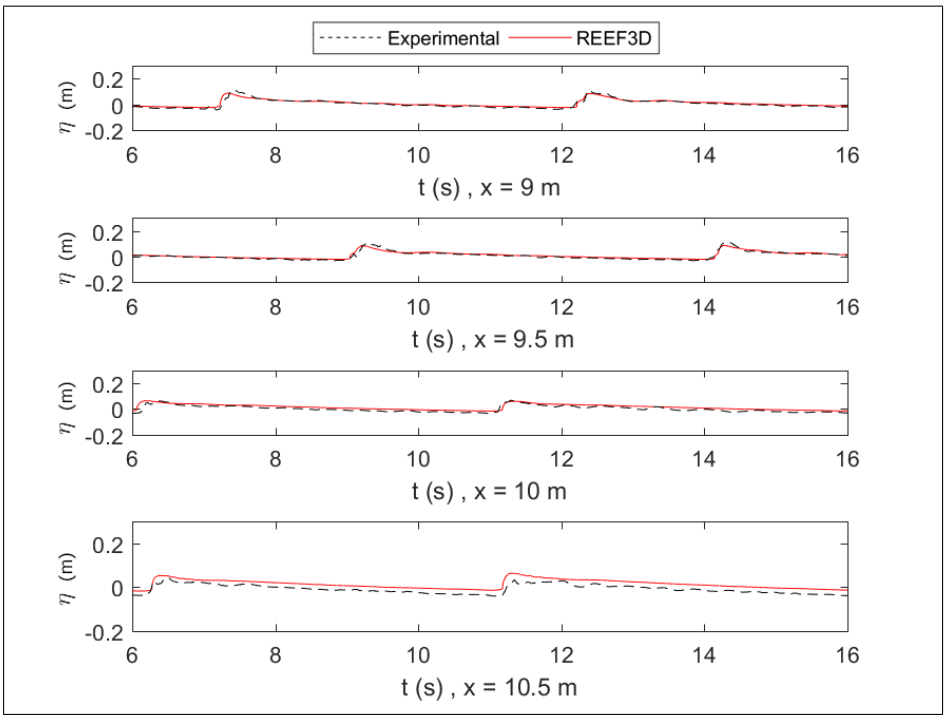

Figure 3.16: Free surface elevation time series comparison at four locations, ($x = 0$) represents the start of the slope

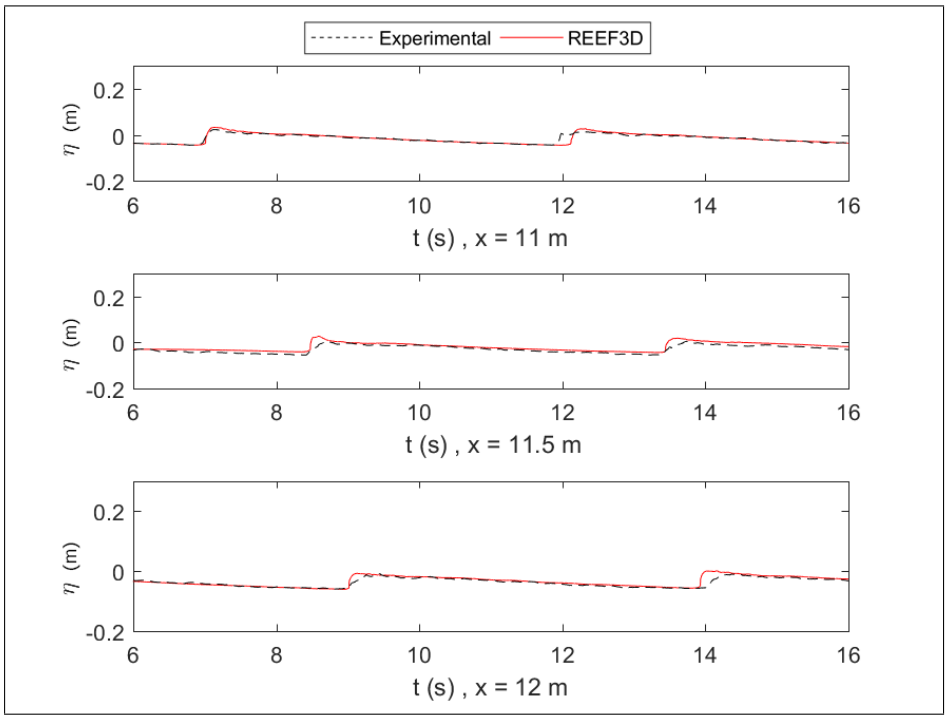

Figure 3.17: Free surface elevation time series comparison at four locations, ($x = 0$) represents the start of the slope

3.3 Case 3: Irregular waves on Irregular slope

In this section, irregular waves are generated on an irregular slope in the experiments of Boers [7] and numerical results are compared with experimental data. This is an important milestone to verify the ability of REEF3D in simulating laboratory waves where parameters are accurately monitored and controlled before testing it with field measurements.

3.3.1 Experimental set-up

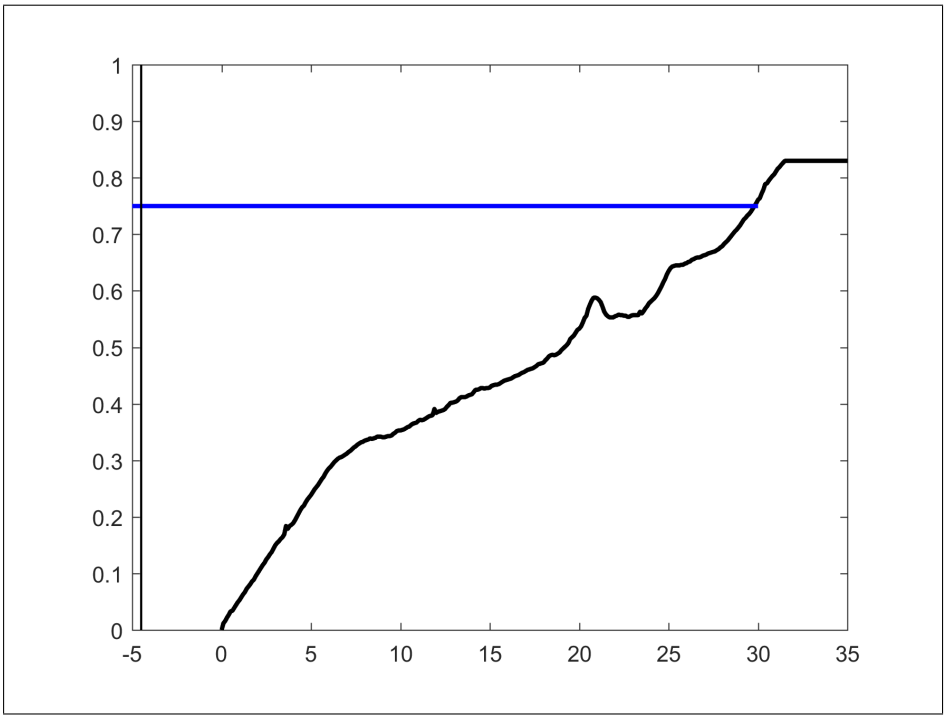

Figure 3.18: Experimental setup from Boers 1995 [7]: The waves are generated 5 m away from the start of the irregular bottom

The experiments of Boers [7] are carried out in the large wave flume at the laboratory of Delft University of Technology. The wave tank is 40 m length, 0.8 m wide and 1.05 m high. The irregular waves were produced by a piston-type wave board allowing for a translatory motion. The waves are generated as a cycle of relatively short signals and this cycle is repeated several times. This method is proven to be effective for determining turbulent motions from ensemble averaging [7]. At the edges of the wave tank there is a reflection compensation system that prevents the re-reflection of waves against the wave board.

An irregular bed profile is constructed from a fill of sand and a smoothed concrete top layer. The profile has a breaker bar and a surf zone trough. The still water level is 0.75 m above the bottom of the flume. Fig 3.18 shows a sketch of the wave tank and the irregular bed.

Time series of the water surface elevations are obtained using wave gauges which is sampled at 20 Hz, from this the wave information is obtained. LDVs was also used to measure the velocities in three directions with a sampling frequency of 100 Hz.

3.3.2 Numerical set-up

A 2D model is used to simulate the Boers experiment since the bed irregularities are only in the cross-shore direction. The numerical domain is 36.3 m length and 1 m height, the still water level is kept at 0.75 m. REEF3D allows for irregular geometry to be simulated, therefore the same beach profile from the experiment was input in the model.

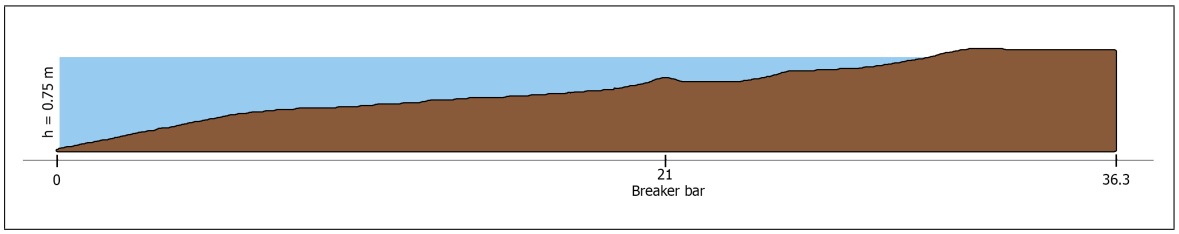

Figure 3.19: Numerical wave tank of Boers case: grid size = 0.005 m, water depth = 0.75 m

Two wave conditions from the experiment will be simulated numerically in this report. The first one is a relatively steep wave with a significant wave height $H_s = 0.157$ m and a peak period of $T_p = 2.05$ s. The second is relatively less steep with $H_s = 0.103$ m significant wave height and $T_p = 3.33$ s peak period. To allow for the comparison of time series, the wave reconstruction method which uses a time series that belong to measurements close to the wave generator is imposed (Section 2.8.3), instead of simply inputting the spectral parameters above.The right boundary is an active absorption beach which prevents reflection of incoming waves by imposing a wave in the opposite direction.

To capture the breaking characteristics accurately, two grid sizes were tested, 0.01 m and 0.005 m and the difference is highlighted.

3.3.3 Results

In this section, the numerical results are compared to the experimental results for both cases of Boers experiment [7]. To better describe the comparison, understanding of the hydrodynamic phenomena and the evolution of the waves temporally and spatially is necessary. Therefore, in addition to the time series of the free surface elevation, information about the energy spectrum of the wave at different locations in the experiment is adopted to describe these changes for both cases.

The energy spectra graphs generated from the numerical simulations have successfully captured the frequencies which have the most energy density. In Figs.3.20 and 3.21 it is noticed that as the wave propagate onshore, the energy amount in the short waves increase due to shoaling and then decrease after breaking. The transformation of energy density from the super harmonic to the sub harmonic region at the end of the numerical tank can also be concluded from the figures.

The difference in energy spectra between the numerical and experiment might be due to the difference in averaging methods used to generate the spectra. It can also be explained by the size of the time series used to generate the spectrum, as the numerical model generate a time series in the order of 1 minute while the experimental time series used can be much longer.

Moreover, spatial snapshot of the waves were obtained from the numerical results of the steep waves case. In Fig. 3.22, the numerical results confirm the shoaling process offshore from the breaker bar in a). In b) and c) the waves can see waves breaking on the bar and on the foreshore respectively.

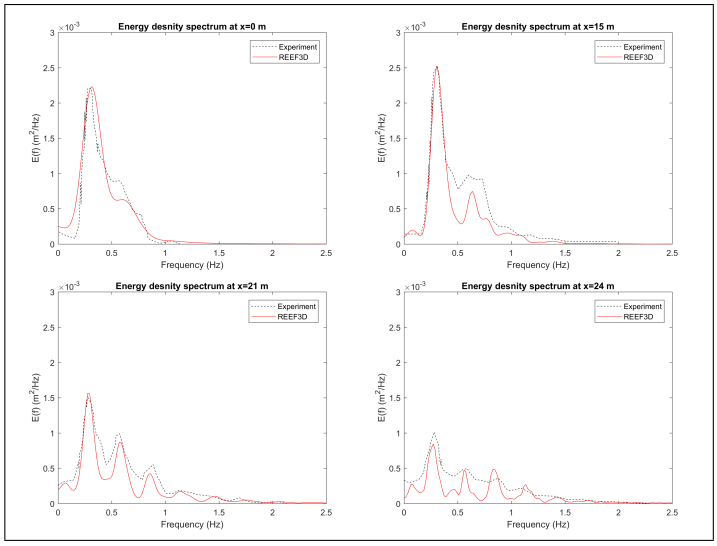

Figure 3.20: Evolution of the energy spectra for the less steep waves ($H_s = 0.103m$, $T_p = 3.33s$)

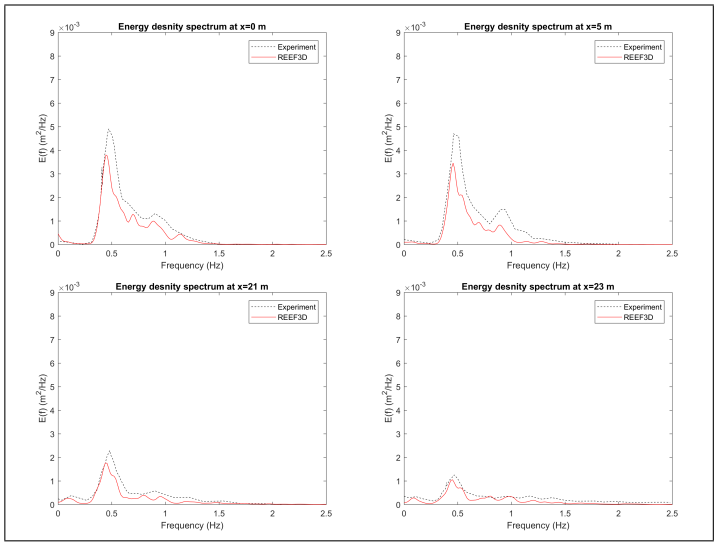

Figure 3.21: Evolution of the energy spectra for the steep waves ($H_s = 0.157m$, $T_p = 2.05s$)

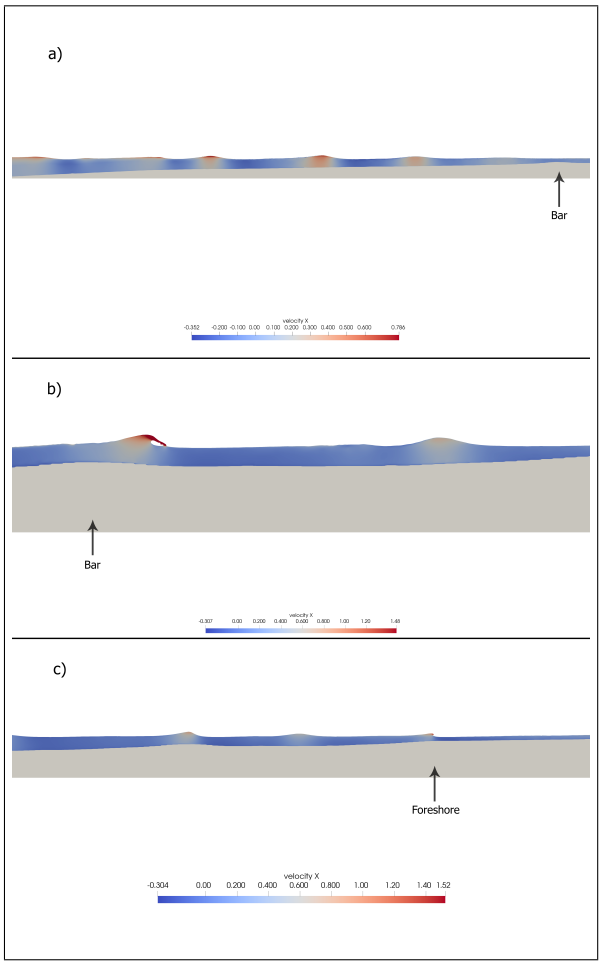

Figure 3.22: Steep waves ($H_s = 0.157m$, $T_p = 2.05s$): a) shoaling of irregular waves b) breaking on the bar c) breaking on the foreshore

Moreover, thanks to the wave reconstruction method, time series of the free surface from the numerical model can be compared to time series from the experiment. Figs. 3.23 and 3.24 shows this comparison for the steep and mild case respectively. For the waves with less steepness, there is a very good matching for all the wave gauges along the profile, However for the case with steep waves, there are some slight differences and specially further onshore after breaking. one reason might be the reflection of infra-gravity waves against the offshore boundary.

The Figs. also highlights the difference of using different grid sizes. Breaking process is very dynamic and involves rapid transformation of wave geometry, that is why using of the smaller grid dx=0.005 m generated more accurate results by resolving the flow and the free surface at more points. The amplitudes and the shape of the wave is better estimated with dx=0.005 m than with dx=0.01 m for both cases.

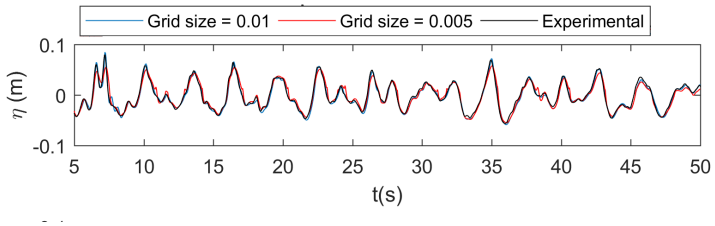

(a) $x = 0m$

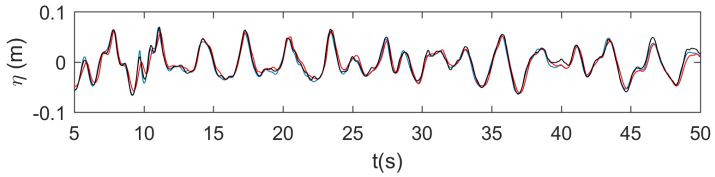

(b) $x = 2m$

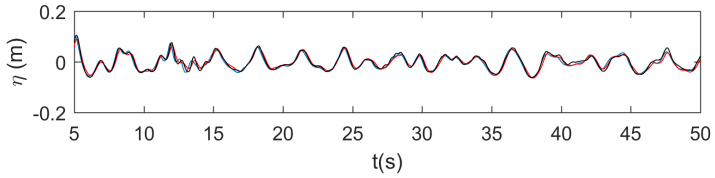

(c) $x = 4m$

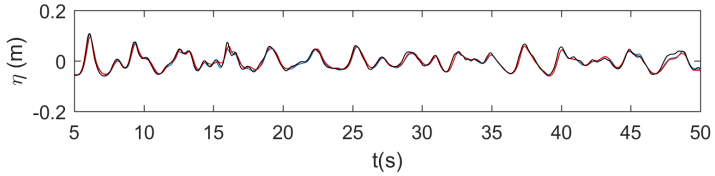

(d) $x = 6m$

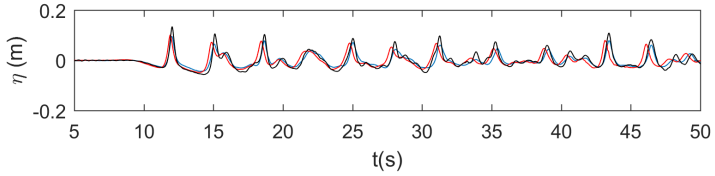

(e) $x = 17.5m$

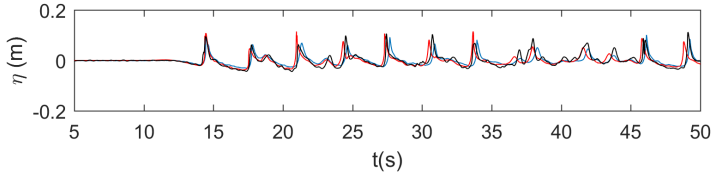

(f) $x = 21.85$

Figure 3.23: Time series of the free surface elevation comparison for the less steep waves case ($H_s = 0.103m$, $T_p = 3.33s$) at six different locations along the irregular slope

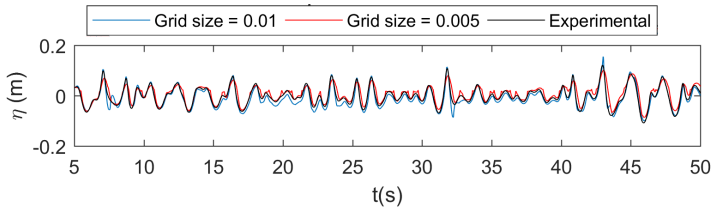

(a) $x = 0m$

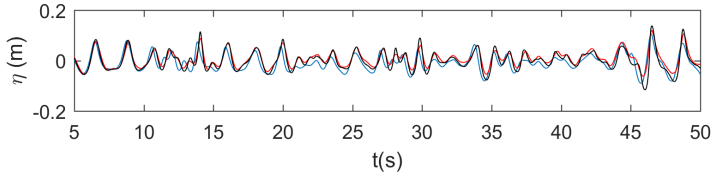

(b) $x = 4m$

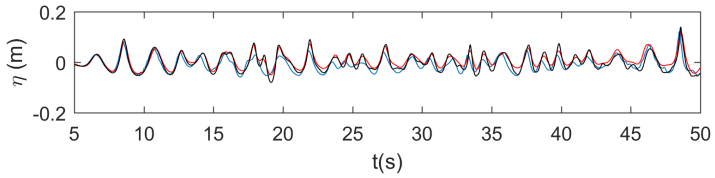

(c) $x = 8m$

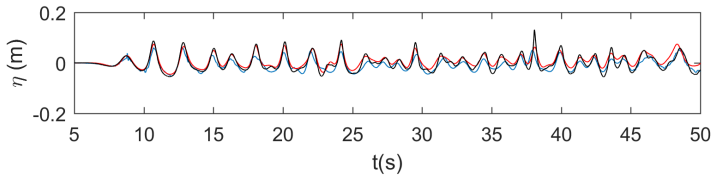

(d) $x = 12m$

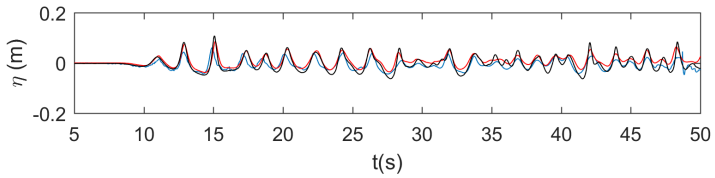

(e) $x = 16m$

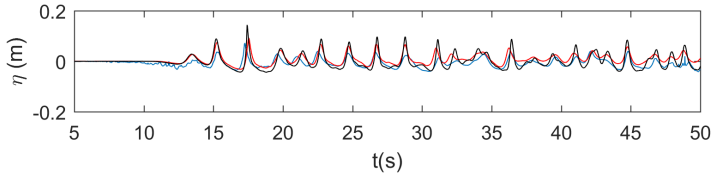

(f) $x = 20$

Figure 3.24: Time series of the free surface elevation comparison for the steep waves case ($H_s = 0.157m$, $T_p = 2.05s$) at six different locations along the irregular slope

3.4 Case 4: Irregular waves on natural topography

Modelling of irregular waves on natural topography beach will be done and compared with ADV field data obtained from Martins et al. [29].

3.4.1 Experimental set-up

A field campaign was carried out in April 2016 at Saltburn-by-the-Sea on the North East coast of England to study wave breaking using different methods.

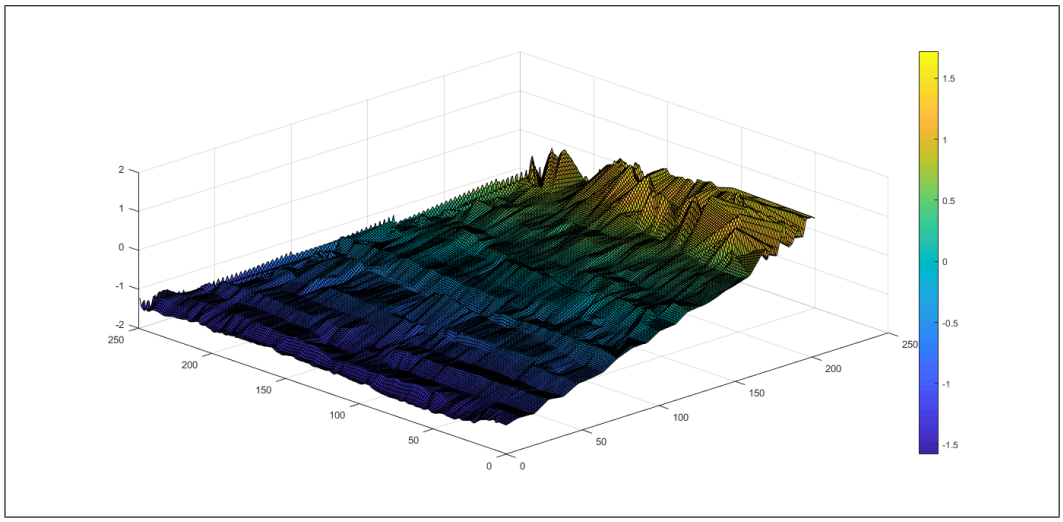

Figure 3.25: Visualization of Saltburn-by-the-Sea beach topography obtained using total station

The wave climate at Saltburn is bi-modal with a combination of northerly swell with a peak period of 9.4 and easterly wind-sea waves with a peak period of 6.2 during the experiments. The bathymetry of the beach was also measured using a total station and RTK GPS during the experiment, see Fig 3.25.
Three ADVs with a sampling frequency of 16 Hz were placed at three different cross-shore locations to measure the time evolution of the free surface and the three dimensional velocities, they were placed 0.2 m above the sea bed (Fig 3.26).
LIght Detection And Ranging (LiDAR) scanners are also employed to measure the water surface to have spatial and temporal information about the evolution of the waves. The spatial and temporal resolution of the LiDAR device is 0.1 and 25 Hz respectively. More information about LiDAR scanners and their deployment for accurate capturing of the shape of the individual breaking waves is presented in Martins et al. [29].

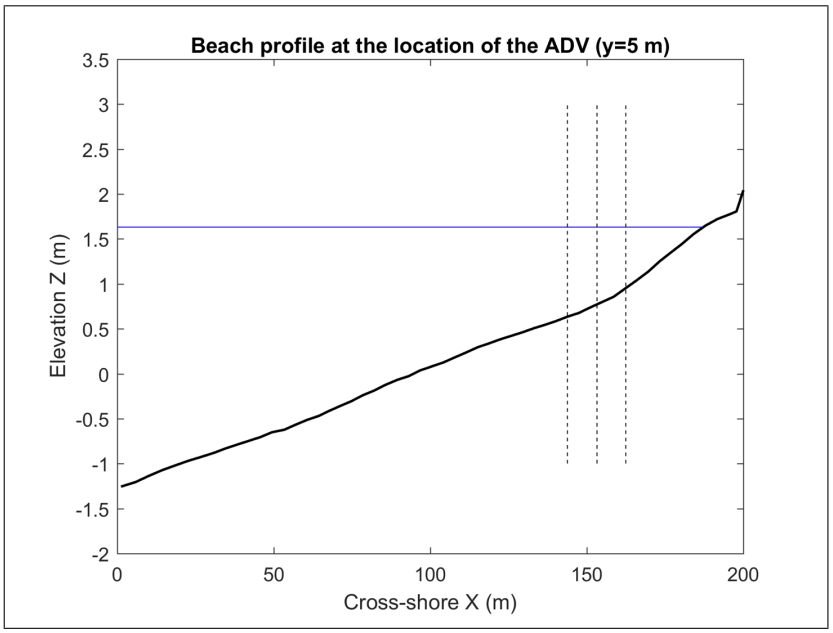

Figure 3.26: Field experiment visualization: Three ADVs are located at $x = 143.8$ m, $x = 153.2$ m and $x = 162.4$ m. The water depth at the location of the most offshore ADV correspond to 2.07 m

The Saltburn beach is characterized as macrotidal, where the tide during the experiment reached a maximum of 5.42 m and a minimum of 3.47 m. Fig 3.27 shows the tidal range and the time at which the measurments taken from the field are used in the simulations. Since the simulation time with the CFD lasts for couple of minutes, the tide and the water depth are assumed constant during this period with values of 1.64 m and 1 m respectively.

3.4.2 Numerical set-up

The simulation of irregular waves on irregular topography to represent the field can be very challenging due to the many uncontrolled variables that play a role in the field. Grid resolution study, influence of wave generation mechanisms and introducing a third horizontal dimension is investigated to arrive at the most accurate representation of the evolution of the waves in the field. The REEF3D results will be compared to both ADV and LiDAR measurments.

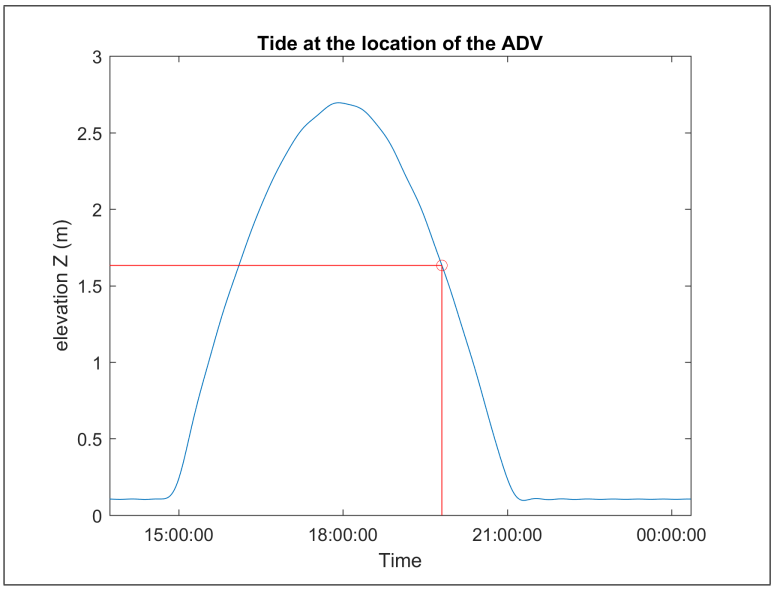

Figure 3.27: Tidal range at the Saltburn-by-the-Sea, the waterlevel at the time selected (19:48:20) for comparison with REEF3D correspond to h = 1.64 m

Base scenario

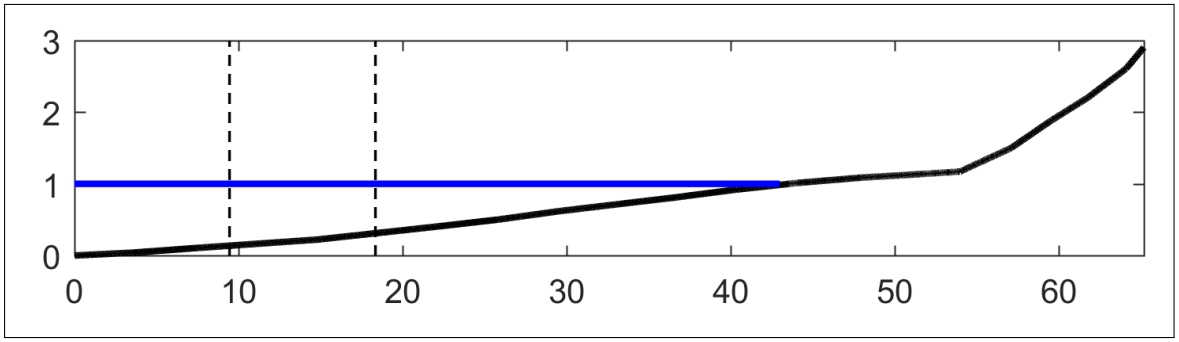

Figure 3.28: Numerical wave tank of base scenario. The dashed lines represent the locations of the middle and onshore ADVs

This numerical setup is set to form a base scenario for the next upcoming cases. A 2D numerical tank (Figure 3.28) with a grid size of 0.007 m with 64 m length and 3 m in height was constructed with a water depth of 1 m.

A Dirichlet boundary is used to generate the irregular waves. The location of the most offshore ADV ($x = 143.8$ m in Fig 3.26) was taken as the start of the wave tank and the dotted lines at $x = 9.45$ m and $x = 18.65$ m are the locations of the middle and onshore ADVs which the REEF3D results are compared to.

Grid optimization

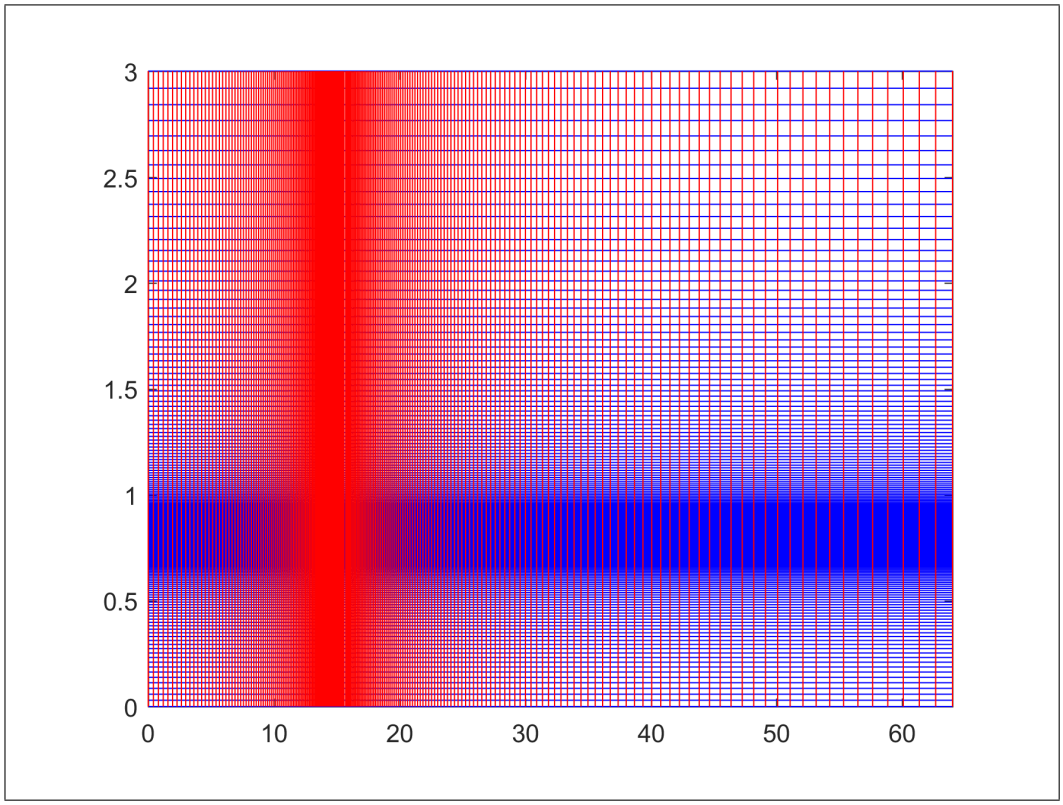

Figure 3.29: Non-uniform grid visualization (400 000 cells, minimum grid size = 13.2 mm)

The base scenario simulation consists of four million cells. This requires a lot of computational time and power. For this reason, non uniform grids are used to refine the mesh in the locations where interesting things happen. This will reduce the computational time without compensating accuracy. Several grid sizes were investigated and the effect on the results is monitored. Table 3.1 shows the number of cells and the minimum grid size of all the simulations done using the non uniform grid option. In

Table 3.1: Non-uniform grid cases

Number of cells	**Minimum grid size**
1.2 million cells	0.007 m
400 000 cells	0.013 m

Fig. 3.29, the mesh resolution is set to increase close to the free surface (z=1 m) to provide more accuracy in the capturing of the free surface. Also refinement is made close to the area where breaking is anticipated (x = 10-20 m) and decreases with distance away from these locations.

Dirichlet vs Relaxation method

In the base scenario, a Dirichlet type boundary condition was imposed which assigns a fixed velocity and water level value for each time step at the incoming boundary. Using the relaxation method, will allow these parameters to be ramped up to their values gradually and is proven to give more accurate representation of the waves, however, increases the number of cells and consequently the computational time. Both types are investigated and the results of the simulations are compared.

2D vs 3D

Waves irregularity in the field is three dimensional. gradients in the longitudinal direction of the bathymetry can play a role in the evolution of the waves. Moreover, waves of different frequencies, periods and directions interact with each other in a complex manner.

A 3D numerical tank (Figure 3.30) is constructed with dimensions of 94 m length, 3 m width, 4 m height and a grid size of dx = 0.05 m and results are compared with the 2D base scenario.

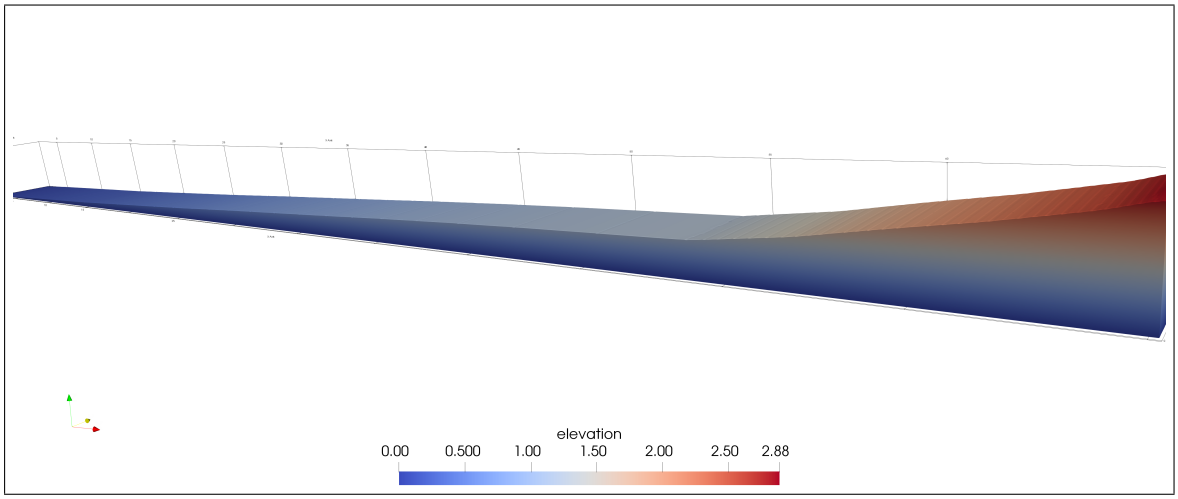

Figure 3.30: Visualization of the bathymetry in the 3D numerical wave tank

3.4.3 Results

Base scenario

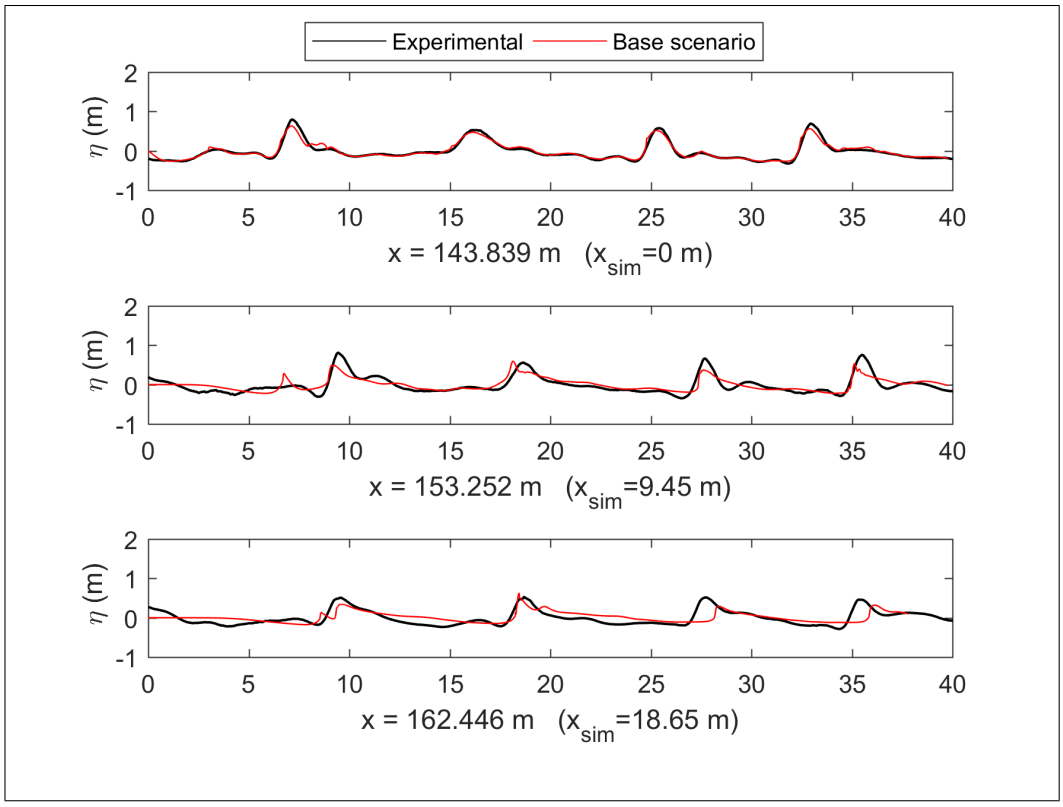

Figure 3.31: Time series of the free surface elevation from REED3D and ADV measurements

Figs 3.31 and 3.32 shows the times series of the free surface elevation for the base scenario and its comparison with ADV and LiDAR measurements respectively. REEF3D accurately estimates the times at which the waves peak and estimates the evolution of the amplitudes in a very good manner.

Generally speaking, REEF3D matches better with the LiDAR than with the ADV measurements. This can be explained from the fact that LiDAR measurements are more reliable than ADV measurements. The LiDAR device does not interact with the water surface, in contrast to the ADV which can alter the results. Moreover, the temporal resolution of the LiDAR is higher than the ADV, with sampling frequency 25 Hz and 16 Hz respectively.

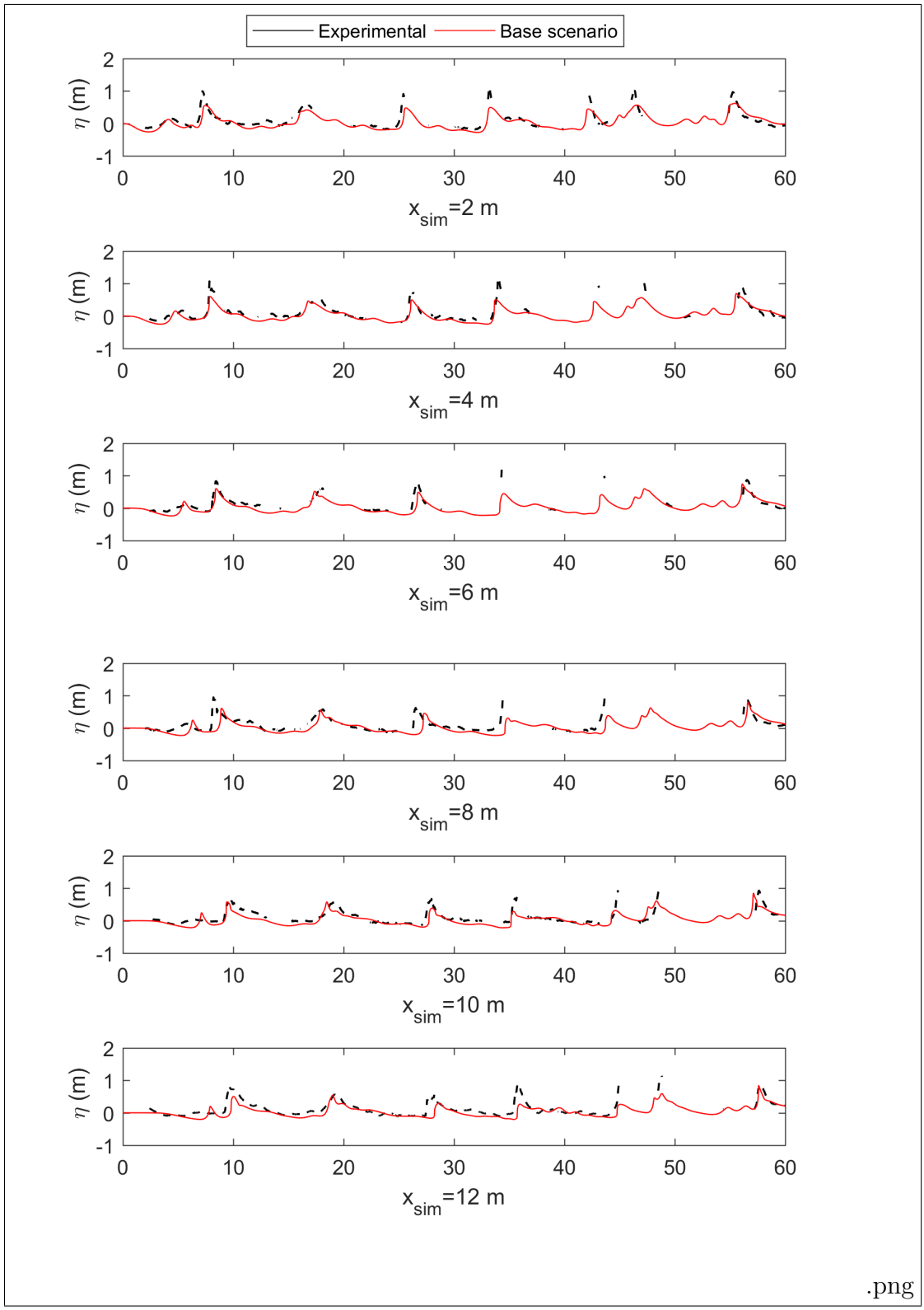

Figure 3.32: Time series of the free surface elevation from REED3D and LiDAR measurements

The situation can be better understood by comparing spatial snapshots of the waves. A cross-shore profile of one wave is captured every one second and compared to measurements from the LiDAR device (Fig 3.33).

The numerical results correctly estimates the shape of the wave during its evolution as it propagates towards the shore. Moreover, the time at which changes happen to the form of the wave corresponds well with the LiDAR measurements.

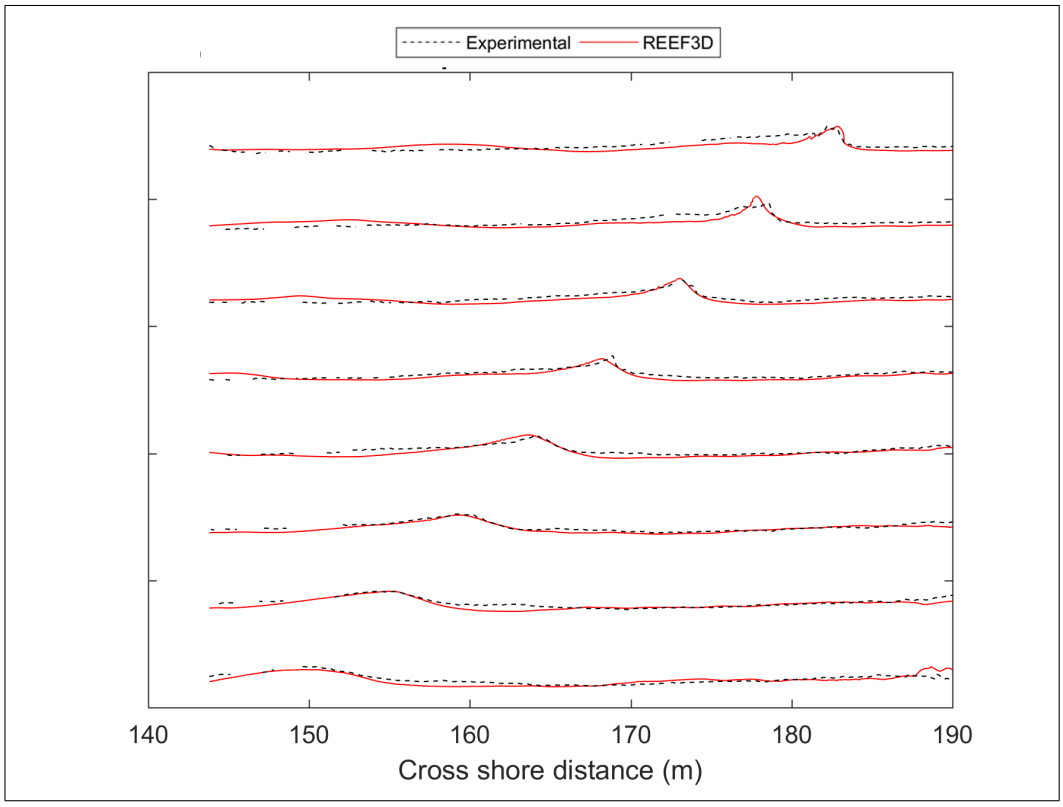

Figure 3.33: Spatial snapshot of the wave profile comparison every 1 second (starting from bottom to top)

Grid optimization

The results of trying different grid size can be considered surprising. In figs 3.34 and 3.35, it is noticed the difference in free surface time series between the simulation with 4 million cells and the simulation with 400 000 cells is negligible. This can be returned to the fact that the grid size close to the area of interest is similar to the base scenario case. Also it is noticed that decreasing the grid size even further (1.2 million cells) does not affect the result.

Thus, it can be concluded that using non-uniform grid with low number of cells can achieve the same accuracy as using uniform grids with many grid cells which can be computationally very expensive.

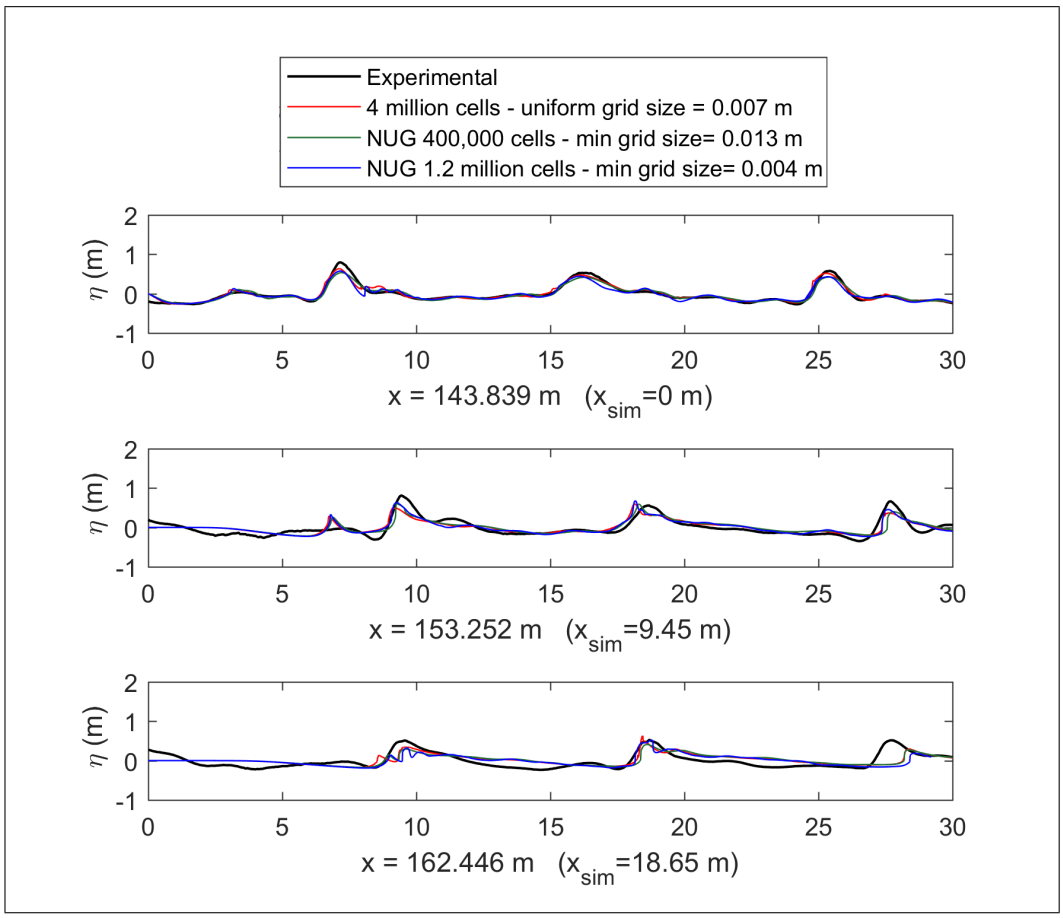

Figure 3.34: Time series of the free surface elevation compared to ADV measurements: Base scenario (uniform grid) vs non-uniform grids

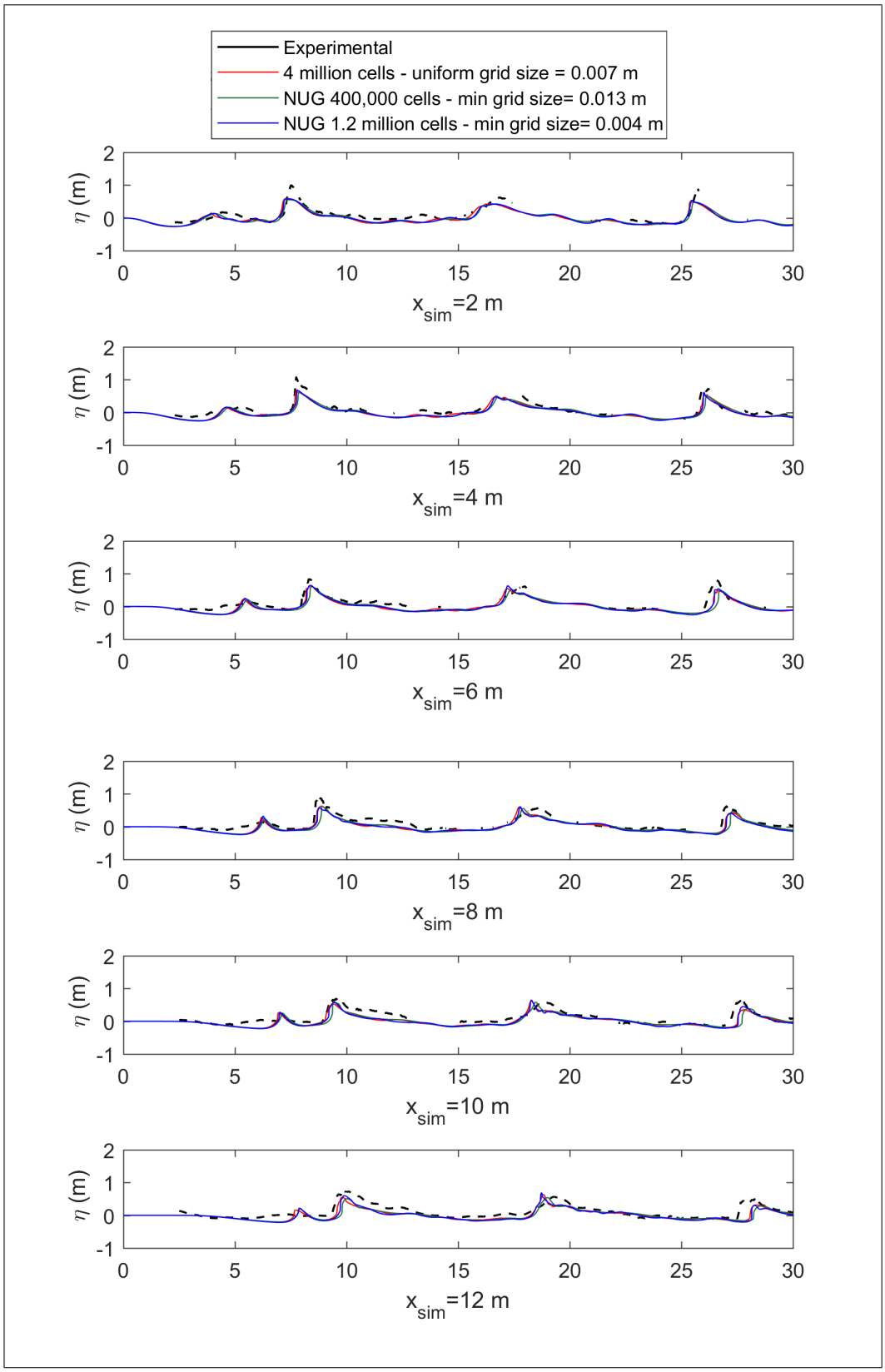

Figure 3.35: Time series of the free surface elevation compared to LiDAR measurements: Base scenario (uniform grid) vs non-uniform grids

Dirichlet vs Relaxation method

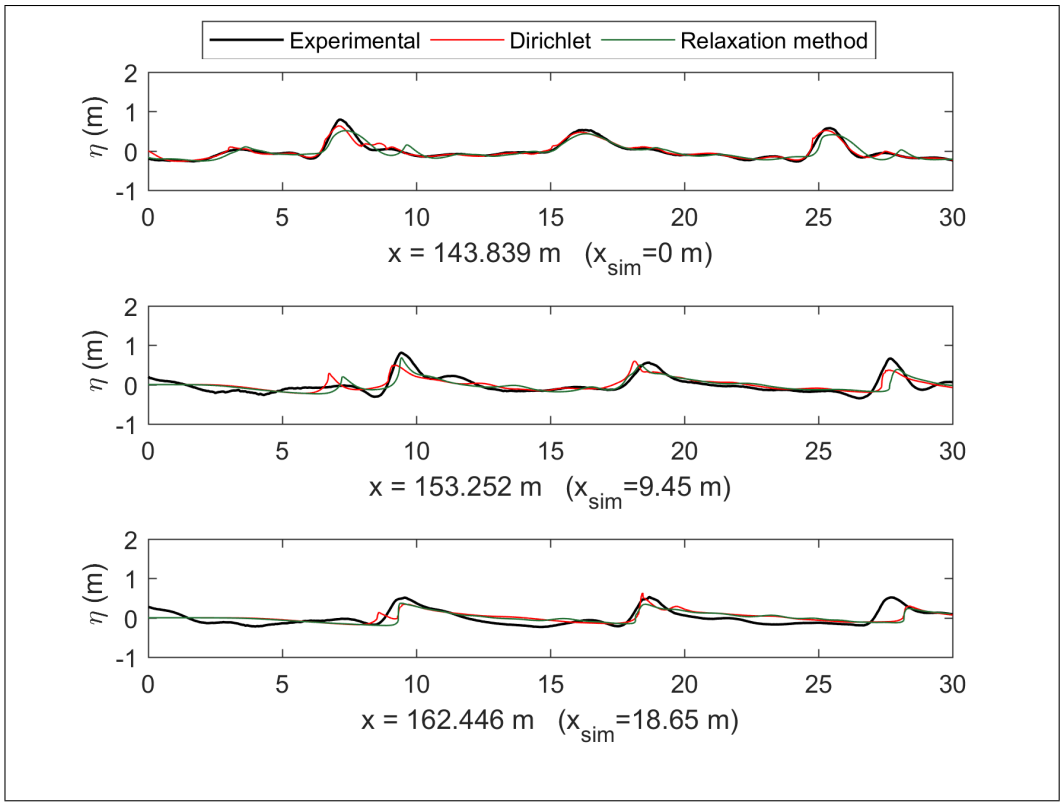

Figure 3.36: Time series of the free surface elevation compared to ADV measurements: Dirichlet vs relaxation method

The results of using the relaxation method in generating the irregular waves did not have a strong effect on the results for both ADV and LiDAR comparisons. The relaxation method worked on gradually changing the values of the initial conditions to the numerical values, and since the numerical values are generated using the wave reconstruction method which is originally obtained from the measurements. The process of gradual changing of the values did not have a strong effect.

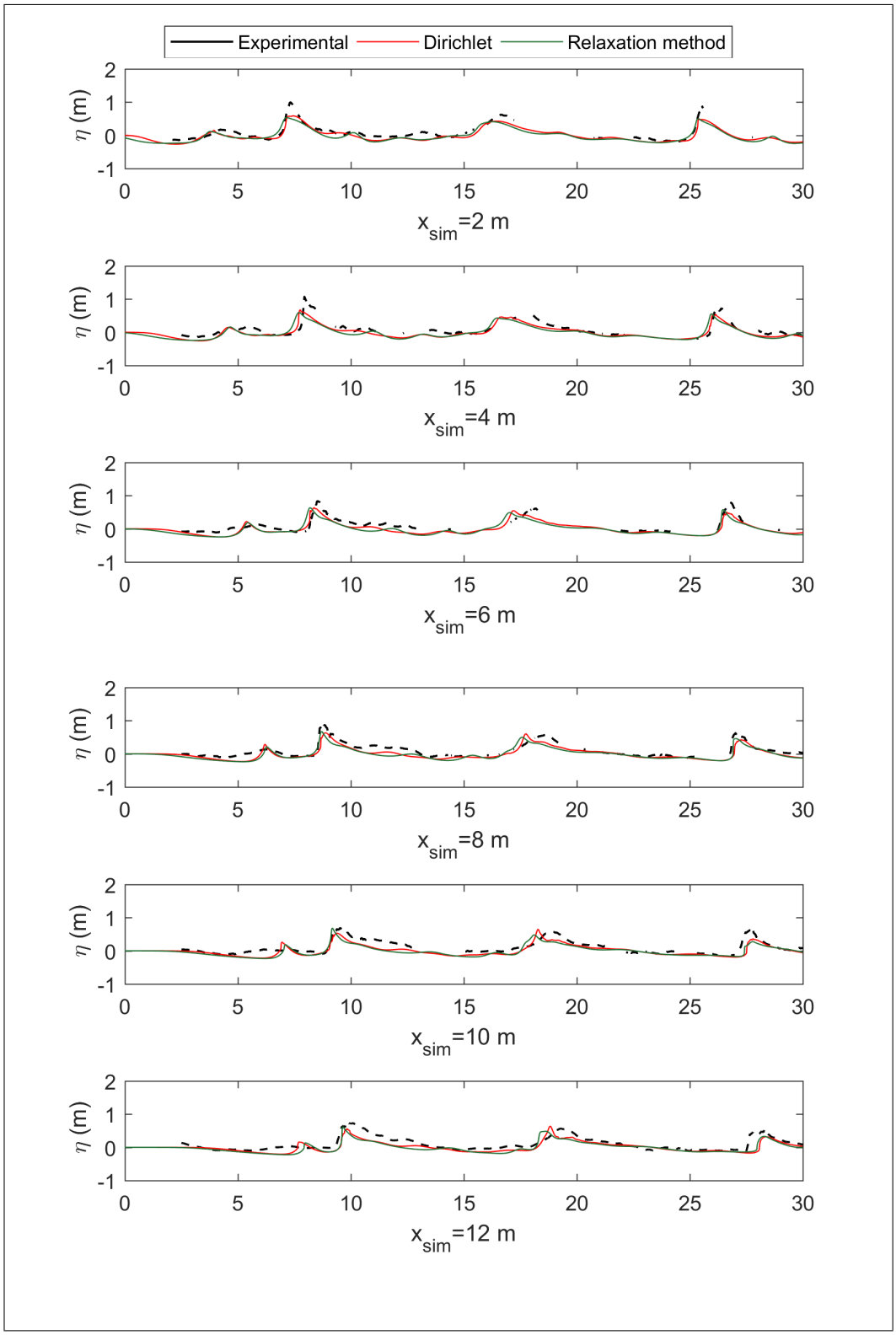

Figure 3.37: Time series of the free surface elevation compared to LiDAR measurements: Dirichlet vs relaxation method

2D vs 3D

The 3D simulation was also very comparable to the 2D one (Figs 3.38 and 3.39). This can be explained by the almost constant bathymetry in the transverse direction (Fig 3.30) or because the width of the numerical tank must be taken sufficiently large to have an effect on the results.

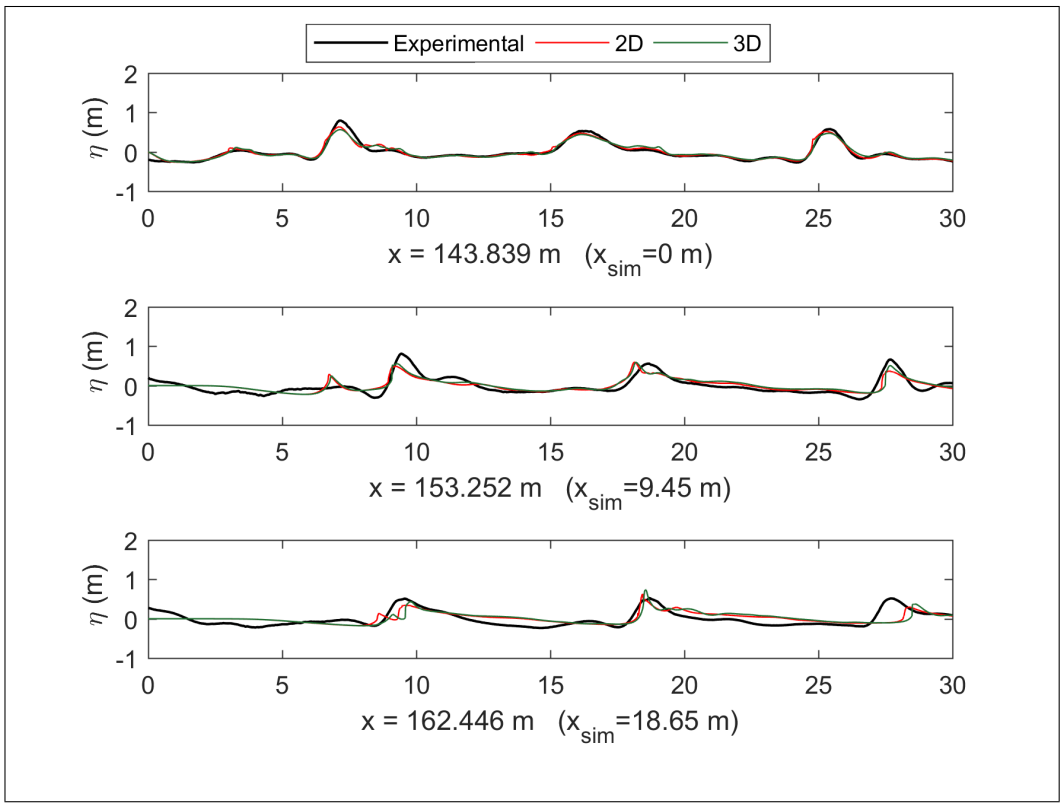

Figure 3.38: Time series of the free surface elevation compared to ADV measurements: 2D vs 3D

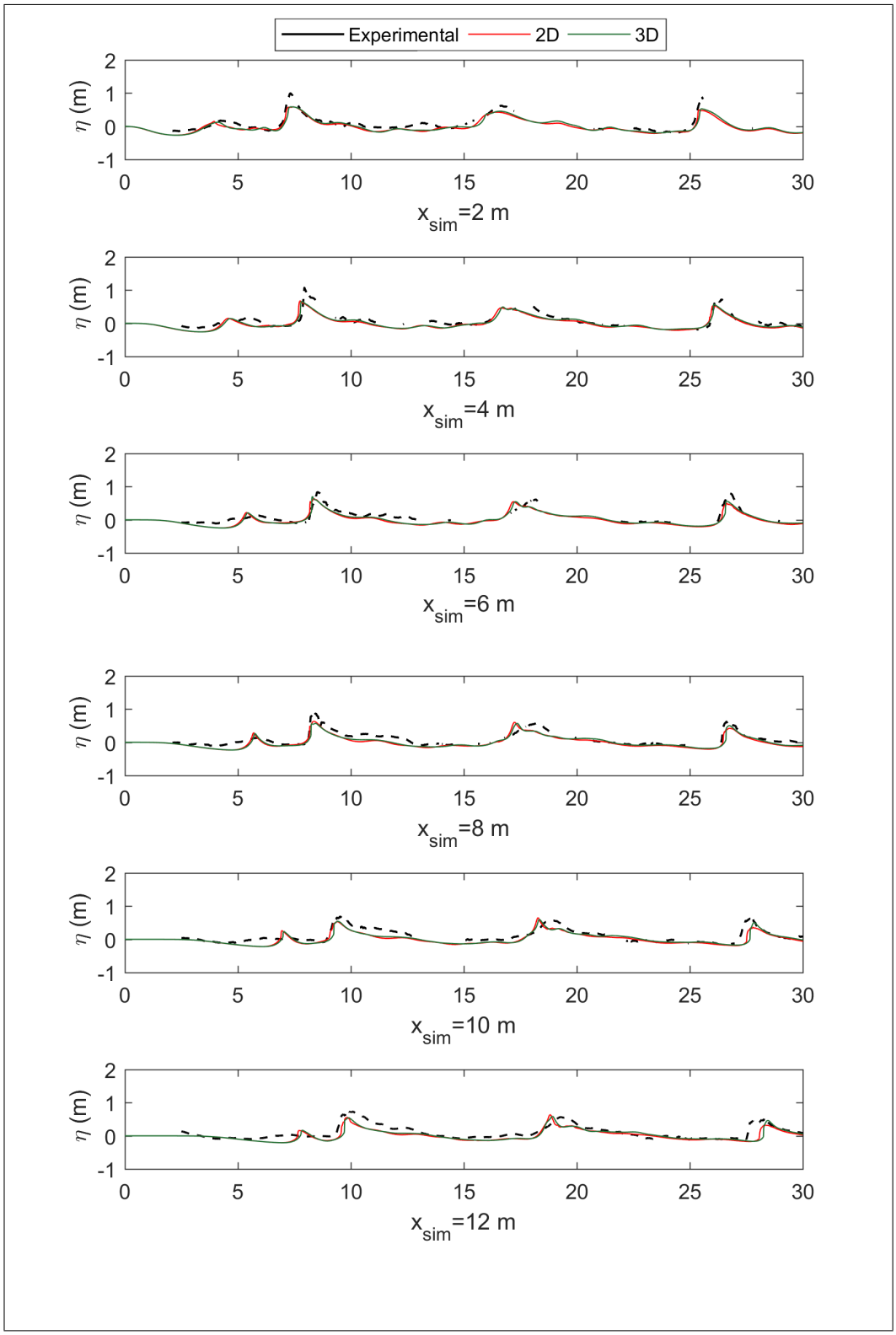

Figure 3.39: Time series of the free surface elevation compared to LiDAR measurements: 2D vs 3D

The 3D simulation however, allowed for visualization of the 3D breaking with pictures, an example is shown in Fig 3.40 where the overturning crest is about to break.

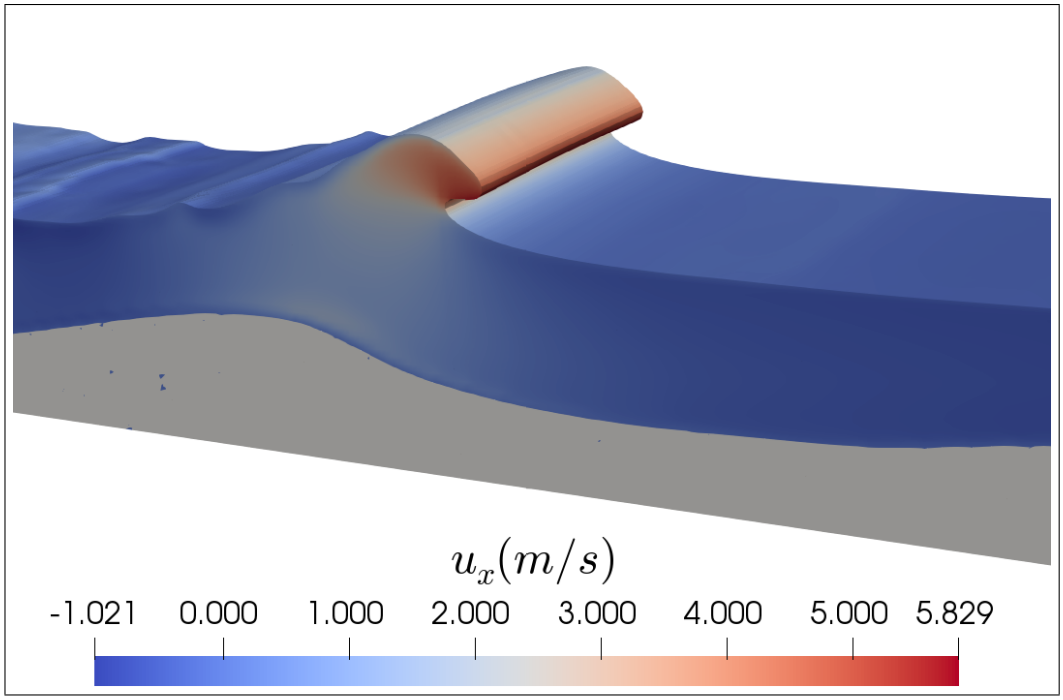

Figure 3.40: Spatial view of 3D breaking obtained from REEF3D

Chapter 4

Outlook

This thesis presented the numerical simulation of four cases to help in understanding the evolution of waves and their breaking behaviour in the coastal zone using REEF3D.

The first case was relatively simple as it represents the propagating of a regular wave on a constant slope and the comparison of the numerical results with the experimental laboratory data. REEF3D results showed a very good matching for both the time series of the free surface and the run-up.

In the second case, REEF3D ability to capture plunging breaking waves was tested. Regular waves were imposed on a plane slope and time series results of the free surface elevation and velocities were found to match very well with laboratory experiments. REEF3D also provided accurate spatial representation of the shape of the plunging wave during the breaking process.

In the third case, the wave reconstruction method was used to generate irregular waves which are identical to a wave signal close to the wave board, thus allowing for time series comparison of the free surface elevation. Two irregular wave cases were simulated and different grid sizes were tried to reach the most accurate representation of the behaviour of the waves on the irregular bottom.

Similarly, wave reconstruction method was used in the fourth case to generate the irregular waves of the field. Non uniform grids were introduced to allow for faster simulations without compensating the accuracy of the results. Moreover, the influence of different wave generation mechanisms and adding a third horizontal dimension is investigated. Results of the free surface elevation and cross-shore profiles were matching to a very great extent with the LiDAR measurements.

Predicting the behaviour of waves in the field can be further improved by allowing the input of more factors that can have impact on the waves for example, wind speed, waves input from more than one direction. In addition to that, more reliable field data must be acquired to allow for further improvement of the model. Overall, REEF3D has proved to be an efficient tool in dealing with complex coastal engineering problems and capturing the waves evolution in the surf zone.

Bibliography

[1] Ankit Aggarwal et al. "Irregular Wave Forces on a Large Vertical Circular Cylinder". In: *Energy Procedia* 94 (2016), pp. 504–516.

[2] Ankit Aggarwal et al. "Numerical study of wave transformation using the free surface reconstruction method". In: ().

[3] Nadeem Ahmad et al. "Three-dimensional CFD modeling of wave scour around side-by-side and triangular arrangement of piles with REEF3D". In: *Procedia Engineering* 116 (2015), pp. 683–690.

[4] Nadeem Ahmad et al. "Three-dimensional numerical modelling of wave-induced scour around piles in a side-by-side arrangement". In: *Coastal Engineering* 138 (2018), pp. 132–151.

[5] Jg A Battjes. "Surf similarity". In: *Coastal Engineering 1974*. 1975, pp. 466–480.

[6] Hans Bihs et al. "A new level set numerical wave tank with improved density interpolation for complex wave hydrodynamics". In: *Computers & Fluids* 140 (2016), pp. 191–208.

[7] Marinus Boers. *Simulation of a Surf Zone with a Barred Beach; Part 1: Wave Heights and Wave Breaking*. 1996.

[8] Judith Bosboom and Marcel JF Stive. *Coastal Dynamics I: Lectures Notes CIE4305*. VSSD, 2012.

[9] GF Carrier and HP Greenspan. "Water waves of finite amplitude on a sloping beach". In: *Journal of Fluid Mechanics* 4.1 (1958), pp. 97–109.

[10] Kuang-An Chang and Philip L-F Liu. "Velocity, acceleration and vorticity under a breaking wave". In: *Physics of Fluids* 10.1 (1998), pp. 327–329.

[11] Mayilvahanan Alagan Chella et al. "Hydrodynamic characteristics and geometric properties of plunging and spilling breakers over impermeable slopes". In: *Ocean Modelling* 103 (2016), pp. 53–72.

[12] Alexandre Joel Chorin. "Numerical solution of the Navier-Stokes equations". In: *Mathematics of computation* 22.104 (1968), pp. 745–762.

[13] *Cnoidal wave*. URL: https://en.wikipedia.org/wiki/Cnoidal_wave. (accessed: 30.04.2018).

[14] Allan P Engsig-Karup et al. "DG-FEM solution for nonlinear wave-structure interaction using Boussinesq-type equations". In: *Coastal Engineering* 55.3 (2008), pp. 197–208.

[15] Robert D Falgout, Jim E Jones, and Ulrike Meier Yang. "The design and implementation of hypre, a library of parallel high performance preconditioners". In: *Numerical solution of partial differential equations on parallel computers*. Springer, 2006, pp. 267–294.

[16] John D Fenton. "The cnoidal theory of water waves". In: *Developments in Offshore Engineering*. Elsevier, 1999, pp. 55–100.

[17] G. Fleit et al. "Investigation of the Effects of Ship Induced Waves on the Littoral Zone with Field Measurements and CFD Modeling". In: *Water* 8.7 (2016), p. 300.

[18] Koichiro Iwata and Toru Sawaragi. "Wave deformation in the surf zone". In: *Memoirs of the Faculty of Engineering, Nagoya University* 34.2 (1982), p. 45.

[19] Niels G Jacobsen, David R Fuhrman, and Jørgen Fredsøe. "A wave generation toolbox for the open-source CFD library: OpenFoam®". In: *International Journal for Numerical Methods in Fluids* 70.9 (2012), pp. 1073–1088.

[20] Guang-Shan Jiang and Chi-Wang Shu. *Efficient implementation of weighted ENO schemes*. Tech. rep. Institute for computer applications in science and engineering Hampton VA, 1995.

[21] Arun Kamath et al. "Cfd simulations of wave propagation and shoaling over a submerged bar". In: *Aquatic Procedia* 4 (2015), pp. 308–316.

[22] Arun Kamath et al. "Energy transfer due to shoaling and decomposition of breaking and non-breaking waves over a submerged bar". In: *Engineering Applications of Computational Fluid Mechanics* 11.1 (2017), pp. 450–466.

[23] Arun Kamath et al. "Evaluating wave forces on groups of three and nine cylinders using a 3D numerical wave tank". In: *Engineering Applications of Computational Fluid Mechanics* 9.1 (2015), pp. 343–354.

[24] A. Kamath et al. "Upstream-Cylinder and Downstream-Cylinder Influence on the Hydrodynamics of a Four-Cylinder Group". In: *Journal of Waterway, Port, Coastal, and Ocean Engineering* 142.4 (2016), p. 04016002. DOI: 10.1061/(ASCE)WW.1943-5460.0000339.

[25] Ying Li and Fredric Raichlen. "Solitary wave runup on plane slopes". In: *Journal of Waterway, Port, Coastal, and Ocean Engineering* 127.1 (2001), pp. 33–44.

[26] Pengzhi Lin and Philip L-F Liu. "A numerical study of breaking waves in the surf zone". In: *Journal of fluid mechanics* 359 (1998), pp. 239–264.

[27] Pierre Lubin et al. "Three-dimensional large eddy simulation of air entrainment under plunging breaking waves". In: *Coastal engineering* 53.8 (2006), pp. 631–655.

[28] Per A Madsen, David R Fuhrman, and Hemming A Schäffer. "On the solitary wave paradigm for tsunamis". In: *Journal of Geophysical Research: Oceans* 113.C12 (2008).

[29] Kévin Martins et al. "High-resolution monitoring of wave transformation in the surf zone using a LiDAR scanner array". In: *Coastal Engineering* 128 (2017), pp. 37–43.

[30] Stefan Mayer, Antoine Garapon, and Lars S Sørensen. "A fractional step method for unsteady free-surface flow with applications to non-linear wave dynamics". In: *International Journal for Numerical Methods in Fluids* 28.2 (1998), pp. 293–315.

[31] Robert L Miller. "Role of vortices in surf zone prediction: sedimentation and wave forces". In: (1987).

[32] Masaru Mizuguchi. "Individual wave analysis of irregular wave deformation in the nearshore zone". In: *Coastal Engineering 1982*. 1982, pp. 485–504.

[33] T Nakagawa. "A new instrument to measure three velocity components of water particles in breaking waves". In: *Journal of Physics E: Scientific Instruments* 16.2 (1983), p. 162.

[34] Dan Naot and Wolfgang Rodi. "Calculation of secondary currents in channel flow". In: *Journal of the Hydraulics Division* 108.8 (1982), pp. 948–968.

[35] United Nations. *Percentage of total population living in coastal areas*. URL: `http://www.un.org/esa/sustdev/natlinfo/indicators/methodology_sheets/oceans_seas_coasts/pop_coastal_areas.pdf`. (accessed: 23.05.2018).

[36] Muk Chen Ong et al. "Numerical simulation of free-surface waves past two semi-submerged horizontal circular cylinders in tandem". In: *Marine Structures* 52 (2017), pp. 1–14.

[37] Stanley Osher and James A Sethian. "Fronts propagating with curvature-dependent speed: algorithms based on Hamilton-Jacobi formulations". In: *Journal of computational physics* 79.1 (1988), pp. 12–49.

[38] Chi-Wang Shu. "Essentially non-oscillatory and weighted essentially non-oscillatory schemes for hyperbolic conservation laws". In: *Advanced numerical approximation of nonlinear hyperbolic equations*. Springer, 1998, pp. 325–432.

[39] *Staggered grid*. URL: https://www.cfd-online.com/Wiki/Staggered_grid. (accessed: 21.05.2018).

[40] Costas Emmanuel Synolakis. "The runup of solitary waves". In: *Journal of Fluid Mechanics* 185 (1987), pp. 523–545.

[41] Francis CK Ting and James T Kirby. "Dynamics of surf-zone turbulence in a strong plunging breaker". In: *Coastal Engineering* 24.3-4 (1995), pp. 177–204.

[42] *Tsunamis*. URL: https://www.nationalgeographic.com/environment/natural-disasters/tsunamis/. (accessed: 25.04.2018).